Promiscuous targeting of cellular proteins by Vpr drives massive proteomic remodelling in HIV-1 infection

Edward JD Greenwood[1*], James C Williamson[1*], Agata Sienkiewicz[1], Adi Naamati[1], Nicholas J Matheson[1], Paul J Lehner[1].

* These authors contributed equally to this work

1. Department of Medicine, CIMR, University of Cambridge, CB2 0XY, UK.

Correspondence: EJD Greenwood, ejdg2@cam.ac.uk (lead contact), JC Williamson, jcw76@cam.ac.uk, PJ Lehner, pjl30@cam.ac.uk

Abstract

HIV-1 encodes four 'accessory proteins' (Vif, Vpr, Vpu and Nef), dispensable for viral replication in vitro, but essential for viral pathogenesis in vivo. Well characterised cellular targets have been associated with Vif, Vpu and Nef, which counteract host restriction and promote viral replication. Conversely, whilst several substrates of Vpr have been described, their biological significance remains unclear. Here, we use complementary, unbiased mass spectrometry-based approaches to demonstrate that Vpr is both necessary and sufficient for DCAF1/DDB1/CUL4 E3 ubiquitin ligase-mediated degradation of at least 38 cellular proteins, causing systems-level changes to the cellular proteome. We therefore propose that promiscuous targeting of multiple host factors underpins complex Vpr-dependent cellular phenotypes, and validate this in the case of G2/M cell cycle arrest. Our model explains how Vpr modulates so many cell biological processes, and why the functional consequences of previously described Vpr targets, identified and studied in isolation, have proved elusive.

Introduction

The HIV-1 'accessory proteins' Vif, Vpr, Vpu and Nef function by binding host proteins and recruiting them to cellular degradation machinery, resulting in depletion of these target substrates (Matheson et al., 2016; Simon et al., 2015; Sugden et al., 2016; Sumner et al., 2017). Some of the targets of Vif, Vpu and Nef, such as Tetherin, APOBEC3 family members and SERINC3/SERINC5, are dominant acting viral restriction factors, and their degradation is therefore thought to enhance *in vivo* viral replication directly. Conversely, the role of the Vpr in enhancing viral replication remains unclear.

Unlike other accessory proteins, Vpr is packaged into nascent viral particles, delivered into newly infected cells, and therefore present in the earliest stages of the viral replication cycle. Even though Vpr does not enhance *in vitro* viral replication in most experimental systems, a number of cellular phenotypes have been ascribed to it – indeed, it has been described as an 'enigmatic multitasker'(Guenzel et al., 2014). For example, expression of Vpr has variously been reported to cause arrest of cycling cells at the G2/M phase, apoptosis, enhancement of HIV gene expression, and stimulation or inhibition of key signalling pathways such as NFκB and NFAT(Ayyavoo et al., 1997; Felzien et al., 1998; Lahti et al., 2003; Re et al., 1995; Roux et al., 2000)

Although the mechanisms by which Vpr causes such complex effects is controversial, most reports agree that they depend on Vpr interacting with a cellular E3 ligase complex containing DCAF1, DDB1

and Cul4 (Dehart and Planelles, 2008; Le Rouzic et al., 2007). As with the other accessory proteins, Vpr is therefore presumed to function by recruiting cellular factors to this E3 ligase complex, resulting in their ubiquitin-dependent degradation. Accordingly, several host factors depleted by Vpr have been identified, but their connection to Vpr-associated cell biological phenotypes is generally unclear, as is their role in regulating viral replication in vivo (Hofmann et al., 2017; Hrecka et al., 2016; Laguette et al., 2014; Lahouassa et al., 2016; Lv et al., 2018; Maudet et al., 2013; Romani et al., 2015; Schrofelbauer et al., 2005; Zhou et al., 2016).

We previously used unbiased quantitative proteomics to map temporal changes in cellular protein abundance during HIV infection of CEM-T4 T-cells, and identify novel targets of Vpu (SNAT1), Nef (SERINC3/5) and Vif (PPP2R5A-E) (Greenwood et al., 2016; Matheson et al., 2015). Nonetheless, known accessory protein targets could only account for a tiny fraction of all the HIV-dependent protein changes observed in our experiments (Greenwood et al., 2016). Given the varied cell biological phenotypes ascribed to Vpr, we hypothesised that it may be responsible for some of the remaining changes. In this study, we therefore undertake a comprehensive analysis of the effects of Vpr on the cellular proteome of HIV-1 infected cells and combine this with further unbiased approaches to identify cellular proteins directly targeted and degraded by Vpr. Our data suggest a new model for the effects of Vpr on cells, in which promiscuous targeting of host factors distinguishes it from other HIV accessory proteins.

Results

Vpr is required for global proteome remodelling in HIV infected cells.

First, we compared total proteomes of uninfected cells with cells infected with either WT HIV or an HIV Vpr deletion mutant (HIV ΔVpr) at an infectious MOI of 1.5 (**Figure 1A**), resulting in approximately 75% infection (**Figure 1B**). Data from this experiment are available, together with the other proteomics datasets presented here, in a readily searchable interactive format in **Table S1**. As expected, amongst the 7,774 quantitated proteins, we observed widespread changes in cells infected with wild-type HIV (**Figure 1C** left panel). Together with known Nef, Vpu and Vif, targets, we saw depletion of previously reported Vpr targets including HLTF (Hrecka et al., 2016; Lahouassa et al., 2016), ZGPAT (Maudet et al., 2013), MCM10 (Romani et al., 2015), UNG (Schrofelbauer et al., 2005), TET2 (Lv et al., 2018), MUS81 and EME1 (Laguette et al., 2014; Zhou et al., 2016). DCAF1, part of the ligase complex used by Vpr to degrade targets was also depleted, consistent with a previous report (Lapek et al., 2017).

In HIV ΔVpr infection (**Figure 1C**, right panel), depletion of Nef, Vpu and Vif targets was maintained. Remarkably, as well as abolishing depletion of known Vpr targets, almost all of the previously uncharacterised protein changes were also reduced or abolished in HIV ΔVpr infection. Whilst 1,944 proteins changed significantly ($q<0.01$) in WT HIV-infected cells, only 41 protein changes (2%) retained significance when cells were infected with HIV ΔVpr. Indeed, principle component analysis showed that cells infected with HIV ΔVpr virus share more similarity on the proteome level with uninfected cell than with cells infected with WT virus (**Figure 1D**).

Incoming Vpr protein alone drives massive cellular proteome remodelling.

Since Vpr enhances expression of other viral proteins (Forget et al., 1998; Goh et al., 1998) (**Figure 1C**), differences between WT and ΔVpr viruses could potentially be explained by secondary changes

81 in expression levels of other proteins, or different rates of progression of WT and ΔVpr viral
82 infections. To eliminate these potential confounders, we next examined the effect of Vpr acting
83 alone. Unlike other HIV-1 accessory proteins, Vpr is specifically packaged into nascent viral particles.
84 We therefore repeated our proteomic analysis using cells exposed to lentiviral particles lacking or
85 bearing Vpr in the presence of reverse transcriptase inhibitors (RTi). This approach excludes all *de*
86 *novo* viral protein expression, focussing on changes induced by incoming Vpr delivered directly by
87 virions (**Figure 2A**). For these experiments, cells were exposed to viral particles at an infectious MOI
88 of 0.5 (determined in the absence of RTi).

89 Strikingly, changes induced by Vpr-containing viral particles phenocopied the Vpr-dependent
90 proteome remodelling seen in HIV infection (**Figure 2B**), with a very high degree of correlation (r^2 =
91 0.67; **Figure 2C**). Taking both experiments together, Vpr is therefore both necessary and sufficient to
92 cause the significant (q<0.01) depletion of at least 302 proteins, and the upregulation of 413 –
93 highlighted in blue and red, respectively (**Figure 2C**). This is a stringent false discovery rate and, in
94 practice, the number of Vpr-dependent changes is almost certainly even higher. Where antibodies
95 were available, we confirmed a proportion of these changes by immunoblot (**Figure S1A-C**).

96 **Cellular proteome remodelling requires interaction with DCAF1 and cellular substrates.**
97 While the function or functions of Vpr remain controversial, in all phenotypic descriptions, Vpr
98 activity is dependent on the interaction between Vpr and the DCAF1/DDB/Cul4 ligase complex,
99 recruitment of which results in ubiquitination and degradation of known Vpr targets by the
100 ubiquitin-proteasome system (Dehart and Planelles, 2008). Therefore, in addition to testing the
101 effect of wild type Vpr protein, we tested a number of previously described mutant Vpr variants (see
102 schematic in **Figure 2A**, results in **Figures 2D & Figure S1F** and additional information in **Figure S1D-**
103 **G**)

104 Since the Q65 residue of Vpr is required for the interaction with DCAF1 (Le Rouzic et al., 2007), we
105 first compared proteome changes caused by a Q65R Vpr mutant with WT Vpr. As predicted, Q65R
106 Vpr was almost completely inactive (**Figure 2D**). We recapitulated this finding by comparing the
107 effects of WT Vpr in control cells, or cells depleted of DCAF1 (**Figure S2A**). ShRNA-mediated
108 depletion of DCAF1 resulted in an approximately 50% reduction in protein abundance of DCAF1
109 (**Figure S2B**). As a proportion of cellular DCAF1 was still expressed, known Vpr effects including
110 degradation of HLTF and upregulation of CCNB1 was partially rather than completely inhibited
111 (**Figure S2C**). Consistent with this, Vpr mediated changes were broadly reduced in magnitude in the
112 DCAF1 knockdown cells (**Figure S2D**). Thus, as with depletion of known Vpr targets, extensive Vpr-
113 dependent proteomic remodelling is dependent on the interaction of Vpr with its cognate
114 DCAF1/DDB/Cul4 ligase. Importantly, depletion of DCAF1 alone did not phenocopy Vpr-mediated
115 proteome remodelling, and the widespread effects of Vpr are therefore unlikely to result from
116 sequestration and/or depletion of DCAF1.

117 Residues E24, R36, Y47, D52 and W54 of Vpr are also required for the recruitment and degradation
118 of previously described Vpr targets, and are reported to form the substrate-binding surface (Hrecka
119 et al., 2016; Selig et al., 1997; Wu et al., 2016). In particular, Y47, D52 & W54 make up a proposed
120 DNA-mimicking motif by which Vpr binds the cellular target UNG2 (Wu et al., 2016). In agreement,
121 the $Vpr_{E24R, R36P}$ and Vpr_{W54R} mutants showed attenuated remodelling of the proteome, while a triple
122 mutant, $Vpr_{Y47A, D52A, W54R}$, was defective for almost all Vpr-dependent protein changes (**Figure 2D**).

123 Global protein remodelling therefore depends on both the substrate binding surfaces of Vpr, and the
124 recruitment of DCAF1, suggesting that this process is mediated by recruitment of Vpr substrates to
125 the DCAF1/DDB1/CUL4 E3 ligase complex, and their subsequent degradation.

126 Vpr causes G2/M arrest in cycling cells, but the mechanism remains contentious (Belzile et al., 2010;
127 Berger et al., 2015; Fregoso and Emerman, 2016; Hohne et al., 2016; Laguette et al., 2014; Liang et
128 al., 2015; Re et al., 1995; Romani et al., 2015; Terada and Yasuda, 2006), as is the connection to the
129 replicative advantage Vpr provides *in vivo.* To investigate this important issue, we took advantage of
130 previously characterised Vpr mutants. Residue S79 of Vpr is required for Vpr-dependent cell cycle
131 arrest (Zhou and Ratner, 2000) (**Figure 2D** and **Figure S1E**). Of the other mutants we tested, Vpr_{Q65R}
132 and $Vpr_{Y47A, D52A, W54R}$ mutants are also unable to cause G2/M arrest, while $Vpr_{E24R, R36P}$ has an
133 intermediate phenotype, and Vpr_{W54R} caused G2/M arrest at wild type levels (**Figure 2D** and **Figure**
134 **S1E**). Strikingly, most Vpr-dependent protein changes were also observed with the Vpr_{S79A} mutant
135 (**Figure 2D**), and are therefore independent of G2/M cell cycle arrest. The presence or absence of
136 G2/M arrest was also a poor correlate of proteomic remodelling across the entire panel of mutants.
137 Cell cycle arrest therefore only explains a minority of Vpr-dependent changes **(Figure 2D)**.

138 To confirm this finding, we examined published datasets/reports describing proteins increased or
139 depleted during different phases of the cell cycle, or in chemically G2/M arrested cells (Fischer et
140 al., 2016; Ly et al., 2015) (**Figure S3**). Compared with cells exposed to Vpr in our study, cells arrested
141 in G2 using a PLK1 inhibitor showed similar regulation of the cyclin family of proteins (**Figure S3B**),
142 but there was little other correlation between these datasets. Thus, whilst some changes in protein
143 levels induced by Vpr may be explained by the effects of cell cycle arrest, proteins regulated by cell
144 cycle in these datasets only account for a small minority of Vpr-dependent changes (**Figure S3A,C,D**).

145 **Vpr directly targets multiple nuclear proteins with DNA/RNA-binding activity.**
146 Vpr has a nuclear localisation and all reported direct Vpr targets are nuclear proteins. Primary Vpr
147 targets are therefore predicted to be nuclear. Conversely, secondary effects resulting from, for
148 example, transcriptional changes, may be distributed across the cell. Analysis of the 302 proteins
149 depleted by Vpr revealed a profound enrichment for proteins that reside in the nucleus (>80%)
150 (**Figure 2E**). This raised the possibility that a large proportion of the proteins depleted by Vpr could
151 be direct targets, as secondary effects should not be limited to the nucleus. Consistent with this,
152 proteins upregulated by Vpr, which are all predicted to be secondary effects, were distributed across
153 multiple compartments. Furthermore, proteins depleted by Vpr were enriched (>70%) for nucleic
154 acid binding activity (**Figure S1G**). Vpr associates with DNA-binding proteins such as UNG via a
155 substrate-binding surface that mimics DNA (Wu et al., 2016). Thus, rather than targeting a small
156 number of cellular proteins for degradation, Vpr may have a much wider range of direct targets, and
157 the structure of the substrate binding surface suggests a possible mechanism for promiscuous
158 recruitment of DNA/RNA-binding cellular proteins.

159 To identify proteins targeted directly by Vpr, we first adopted a co-immunoprecipitation approach
160 (**Figure S4**). Cells were transduced with a 3xHA tagged Vpr lentivirus in the presence of an shRNA to
161 DCAF1 and the pan-cullin inhibitor MLN4924, to minimise substrate degradation and enhance co-
162 immunoprecipitation. Factors specifically co-immunoprecipitated in the presence of Vpr are
163 expected to include direct Vpr targets and, accordingly, were enriched for proteins depleted (rather
164 than increased) in the presence of Vpr (**Figure S4B,D,E**). However, the co-IP was dominated by

165 DCAF1, a stable binding partner of Vpr, identified with a signal intensity 2 orders of magnitude
166 greater than all other proteins (**Figure S4C**). This is despite the knockdown of DCAF1 in these cells,
167 which reduces the DCAF1 protein abundance by approximately 50% (**Figure S2B**). In addition, at
168 least 13 proteins co-immunoprecipitating with Vpr are reported to physically interact with DCAF1
169 alone (Coyaud et al., 2018; Guo et al., 2016; Hossain et al., 2017), of which 11 are not regulated by
170 Vpr, and two, CEP78 and IQGAP2, are upregulated by Vpr, explaining their presence in this list of
171 proteins.

172 This mismatch between the high abundance of DCAF1 and the relatively low abundance of direct Vpr
173 targets for degradation is consistent with previous reports, which have also found that MS-IP based
174 techniques are ideal for the identification of the cellular machinery co-opted by viral proteins, but
175 often struggle to identify cellular targets, which interact transiently and in competition with each
176 other (Jager et al., 2011; Luo et al., 2016). We therefore adopted an alternative, pulsed-Stable
177 Isotope Labelling with Amino Acids in Cell Culture (pulsed-SILAC) approach to identify host proteins
178 specifically destabilised within 6 hrs of exposure to Vpr (**Figure 3A**). This technique is directly
179 analogous to a traditional pulse-chase experiment using radiolabelled methionine/cysteine, but
180 allows a global, unbiased analysis of potential cellular targets (Boisvert et al., 2012). Since proteins
181 are fully labelled prior to exposure to Vpr, differences in abundances of labelled proteins between
182 conditions exclusively reflect changes in protein degradation rates.

183 Six hours after exposure to Vpr, the stability of most proteins was unchanged (**Figure 3B,** top panel).
184 However, a subset of proteins depleted by Vpr were already destabilised, consistent with Vpr-
185 dependent proteasomal degradation. These 27 proteins, including HLTF, are therefore represent
186 direct targets for Vpr-mediated depletion (**Figure 3C**). After 24 hours of exposure to Vpr, changes in
187 protein stability reflected overall changes in protein abundance caused by Vpr in other experiments
188 (**Figure 3B,** lower panel), including proteins with increased as well as decreased stability. These
189 changes are therefore indicative of both direct and indirect Vpr targets.

190 Combining all orthogonal approaches - whole cell proteomics to identify proteins depleted by Vpr in
191 the context of viral infection or Vpr protein alone delivered in viral particles, MS co-IP with epitope
192 tagged Vpr, and pulsed-SILAC based identification of proteins post-translationally degraded by Vpr -
193 we have identified at least 38 direct targets for Vpr-dependent degradation (**Figure 3D**). Vpr is both
194 necessary and sufficient for depletion of these proteins, which are either bound by Vpr, or
195 destabilised within 6 hours of Vpr exposure (or both). In practice, this list very likely underestimates
196 the true number of direct Vpr targets, as several known targets of Vpr behaved appropriately, but
197 beyond the statistical cut-offs used to derive this table (**Figure S4F**). It is also limited to proteins
198 expressed in this T-cell model.

199 **Novel Vpr targets SMN1, CDCA2 and ZNF267 contribute to G2/M cell cycle arrest.**
200 Several cellular phenotypes have been described for Vpr, including G2/M arrest, transactivation of
201 the HIV LTR, and modulation of cellular signalling pathways such as NFκB and NFAT arrest (Bolton
202 and Lenardo, 2007; Gummuluru and Emerman, 1999; Hohne et al., 2016; Liang et al., 2015; Liu et al.,
203 2014; Muthumani et al., 2006; Rogel et al., 1995). The mechanisms responsible for these phenotypes
204 are controversial. Wide-scale proteome remodelling by Vpr, and direct targeting of multiple
205 proteins, suggests a model in which Vpr interacts with diverse cellular proteins and pathways,
206 resulting in cumulative or redundant effects on cellular phenotypes. This model does not contradict

207 any single mechanism, but suggests that several are involved, with potential variability between
208 different cell types and experimental systems.

209 To test this model, we investigated the best-described phenotype for Vpr, cell cycle arrest at the
210 G2/M phase. We hypothesised that differential depletion of cellular proteins by different Vpr
211 mutants tested in **Figure 2**, which displayed a spectrum of capacity to cause G2/M arrest, would
212 highlight proteins whose depletion resulting in this cellular phenotype. We first examined proteins
213 with a published connection to Vpr-medated G2/M arrest, MCM10, MUS81 and EME1. MCM10 is
214 reported to be directly degraded by Vpr, resulting in cell cycle arrest (Romani et al., 2015). Vpr
215 mediated depletion of MUS81 and EME1 was proposed to be a consequence of Vpr interaction with
216 SLX4 (Laguette et al., 2014), another proposed mechanism of Vpr mediated G2/M arrest, though one
217 that has been subject to conflicting reports (Berger et al., 2015; Fregoso and Emerman, 2016; Zhou
218 et al., 2016). In our system, of these three proteins, only the depletion of MCM10 showed a strong
219 correlation with the extent of G2/M arrest caused by the different mutants (**Figure 4A**). As
220 previously described (Romani et al., 2015), we found RNAi depletion of MCM10 by RNAi to be
221 sufficient to cause accumulation of cells at G2/M (**Figure 4B & 4C**).

222 We therefore interrogated our Vpr mutant dataset (**Figure 2**) for other direct Vpr targets (**Table 1)**
223 which, like MCM10, correlated with the extent of G2/M arrest. In total, we identified 14 targets with
224 a significant relationship ($p < 0.05$ in a linear regression analysis) **(Figure 4D)**. Next, we tested
225 whether shRNA-mediated depletion could phenocopy Vpr-dependent cell cycle arrest at G2/M
226 (**Figure 4D)**. Depletion of 3 Vpr targets: SMN1, CDCA2 and ZNF267 caused G2/M arrest (**Figure 4D**
227 **&E**), and these phenotypes were confirmed with a second shRNA (**Figure 4G**). Thus, several Vpr
228 targets contribute independently to G2/M cell cycle arrest, consistent with a model whereby
229 depletion of multiple cellular proteins underpin the various phenotypes associated with Vpr
230 expression.

231 **Some Vpr targets are conserved across primate lentiviruses, but massive cellular proteome**
232 **remodelling is unique to the HIV-1/SIVcpz lineage.**
233 Targeting of key cellular proteins such as BST2 or the APOBEC3 family is conserved across multiple
234 lentiviral lineages, demonstrating the *in vivo* selective advantage of these interactions. We therefore
235 tested a diverse panel of lentiviral Vpr proteins to determine if they shared activity with the NL4-3
236 Vpr variant used in all the experiments above. We included Vpr variants from primary isolates of
237 HIV-1 from two distinct cross-species transmissions from apes to humans (Group M and Group O), in
238 addition to a closely related SIVcpz variant. We also tested Vpr variants from divergent primate
239 lineages, including HIV-2, SIVsmm, SIVagm and SIVrcm (**Figure 5A** and **Figure S5A &S5B**). In addition
240 to Vpr, which is present in all primate lentiviruses, viruses of some lineages also bear Vpx, a gene
241 duplication of Vpr. Since depletion of some substrates and cellular functions switches between Vpr
242 and Vpx in lineages encoding this accessory gene (Fletcher et al., 1996; Lim et al., 2012), we also
243 included a Vpx variant from HIV-2.

244 Extensive Vpr-dependent remodelling of the cellular proteome was conserved across the HIV-
245 1/SIVcpz lineage (**Figure 5B** – top row). Whilst Vpr variants from other lineages showed a narrower
246 set of changes, depletion of some proteins, particularly those most heavily depleted by HIV-1, was
247 conserved by Vpr variants across multiple lineages (**Figure 5B**,**C**). Depletion of selected proteins for
248 which commercial antibody reagents were available was readily confirmed by immunoblot of cells

249 transduced with an overlapping panel of Vpr variants (**Figure 5D**). These conserved targets of direct
250 Vpr-mediated degradation are likely to provide an *in vivo* replicative advantage for all primate
251 lentiviruses.

252 While none of the identified HIV-1 Vpr targets were degraded by the HIV-2 Vpx (HIV-2_{ROD}) tested, we
253 noted a shared ability of HIV-2 Vpx and SIVagm Vpr to deplete TASOR, a critical component of the
254 Human Silencing Hub (HuSH) transcription repressor complex (Tchasovnikarova et al., 2015) (**Figure**
255 **S5C**). Whilst this manuscript was in preparation, two other groups independently discovered and
256 reported Vpx-mediated depletion of TASOR (Chougui et al., 2018; Yurkovetskiy et al., 2018). The
257 HuSH complex mediates position-dependent transcriptional repression of a subset of lentiviral
258 integrations, and we previously showed that antagonism of HuSH is able to potentiate HIV
259 reactivation in the J-LAT model of latency (Tchasovnikarova et al., 2015). As predicted, Vpx-VLPs
260 phenocopied the effect of RNAi-mediated TASOR depletion on reactivation of the HuSH-sensitive J-
261 LAT clone A1 (**Figure S5D**).

262 Previous reports (Chougui et al., 2018; Yurkovetskiy et al., 2018) were conflicted on the conservation
263 of TASOR depletion across Vpr variants. With some exceptions, most primate lentiviruses can be
264 categorised into 5 lineages (**Figure S5E)**, of which two encode Vpx. The previously described
265 canonical function of Vpx is the degradation of SAMHD1 (Hrecka et al., 2011; Laguette et al., 2011).
266 Two lentiviral lineages lack Vpx, but use Vpr to degrade SAMHD1, while the HIV-1/SIVcpz lineage
267 lacks SAMHD1 antagonism (Lim et al., 2012). We considered that TASOR antagonism may follow the
268 same pattern, and thus tested Vpx proteins from both Vpx bearing lineages, and representative Vpr
269 variants from lineages that use Vpr to degrade SAMHD1. All of these proteins were able to deplete
270 TASOR in Vpx/Vpr transduced cells (**Figure S5F**). Antagonism of SAMHD1 and TASOR therefore follow
271 the same pattern.

272 While the targeting of some substrates was conserved across Vpr varients from multiple lineages, we
273 did not observe broad proteome remodelling outside the HIV-1/SIVcpz lineage. However, in the
274 experiment described in **Figure 5A** an HIV-1 based lentiviral transduction system was used. Of the
275 Vpr and Vpx variants tested, only Vpr proteins from the HIV-1/SIVcpz alleles are efficiently packaged.
276 In these cases, cells receive both incoming and *de novo* synthesized Vpr, while in the case of other
277 variants tested, only *de novo* synthesized Vpr is present. There is therefore a time-lag of at 18-24
278 hours for viral entry, reverse transcription, integration and de novo synthesis of protein to begin. As
279 such, the more limited proteome remodelling seen in Vpr variants could reflect a lack of time for
280 such changes to occur.

281 In order to account for this, we carried out an experiment in which cells were transduced with Vpr or
282 Vpx from the primary HIV-2 isolate 7312a and assayed 48 hours to 96 hours post-transduction
283 (**Figure 5E**), allowing time for additional changes to develop after *de novo* Vpr/Vpx synthesis. Even at
284 96 hours post transduction, HIV-2 Vpr showed very limited changes. The majority of these changes
285 consisted of the depletion of proteins also targeted by HIV-1 Vpr (**Figure 5F** left panel).

286 Curiously, 7312a HIV-2 Vpx also depleted several proteins modulated by HIV-1 Vpr (**Figure 5F –** right
287 panel), including direct targets for HIV-1 Vpr mediated degradation, BBX, HASPIN and ARHGAP11A.
288 Some proteins were degraded by both HIV-2 Vpr and Vpx, while others were only degraded by the
289 Vpx of this isolate. In lentiviral strains and/or lineages that encode both Vpr and Vpx, responsibility

290 for degrading certain targets of HIV-1 Vpr is therefore shared between Vpr and Vpx, further
291 emphasising their *in vivo* importance. Conversely, global proteome remodelling is therefore unique
292 to Vpr variants of the HIV-1/SIVcpz lineage. This activity may help explain why viruses from this
293 lineage appear to be more pathogenic than other primate lentiviruses (Greenwood et al., 2015;
294 Keele et al., 2009), particularly given the potential to drive these changes in Vpr-exposed but
295 uninfected bystander cells.

296 Discussion

297 Proteomic analyses of cells infected with viruses from different orders have revealed widespread
298 and varied changes to the cellular proteome (Diamond et al., 2010; Ersing et al., 2017; Greenwood et
299 al., 2016; Weekes et al., 2014). While these changes are presumed to be multifactorial, in the case of
300 HIV-1 infection, our data show that the majority of changes can be attributed to the action of a
301 single viral protein, Vpr. We propose that this massive cellular proteome remodelling consist of
302 firstly, the direct targeting of multiple cellular proteins for proteosomal degradation via the
303 DCAF1/DDB1/CUL4A E3 ligase complex, followed by resulting secondary effects on other proteins.
304 While many of the changes caused by Vpr are secondary, they occur within the physiological
305 timeframe of productive infection (Murray et al., 2011; Perelson et al., 1996), and are therefore
306 relevant to our understanding of the HIV-1-infected cell. Further, we have recently mapped changes
307 to the cellular proteome in HIV-1 infected primary T-cells and confirmed that the Vpr-mediated
308 changes in our CEM-T4 model represent the majority of changes in primary cells (Naamati et al.,
309 2018).

310 Before this study, the list of direct Vpr targets was already extensive. We have confirmed here Vpr-
311 mediated depletion of the previously described Vpr targets HLTF (Hrecka et al., 2016; Lahouassa et
312 al., 2016), ZGPAT (Maudet et al., 2013), MCM10 (Romani et al., 2015), UNG2 (Schrofelbauer et al.,
313 2005), TET2 (Lv et al., 2018), MUS81 and EME1 (Laguette et al., 2014; Zhou et al., 2016), while
314 SMUG1 (Schrofelbauer et al., 2005) and PHF13 (Hofmann et al., 2017) were not detected in our
315 model T-cell line. By analogy with other HIV accessory proteins, it might have been predicted that
316 this list of Vpr targets would be nearly complete. Instead, we show here that it is only the tip of the
317 iceberg.

318 While surprising, the ability of Vpr to degrade multiple cellular factors may be explained by the
319 biology of this small protein. Mechanistically, depletion of multiple proteins with nucleic acid binding
320 properties is consistent with known structural determinants of Vpr substrate recruitment. From the
321 functional viewpoint, while HIV-1 has three accessory proteins (Vpu, Nef and Vif) to aid viral
322 replication and counteract host defences in the late stages of the viral replication cycle, Vpr is the
323 only HIV-1 accessory protein specifically packaged in virions. Multiple targets may therefore be
324 required both to protect incoming virions from cellular factors, and to prime newly infected cells for
325 productive viral replication.

326 This work does not represent the first attempt to use unbiased proteomics analysis to characterise
327 Vpr function. In general, previous studies have used single proteomic experiments or methods to
328 identify candidate proteins that either interact with, or are depleted by, Vpr, with individual proteins
329 followed up using targeted immunoreagents. For example, Vpr binding partners were identified by
330 Jager *et al.* (Jager et al., 2011) and Hrecka *et al.* (Hrecka et al., 2016) using IP-MS. Amongst these
331 proteins, Jager *et al.* did not determine whether any were depleted. Conversely, Hrecka *et al.*

332 (Hrecka et al., 2016) focussed on the single target protein, HLTF, and found it to be depleted by Vpr.
333 Similarly, Lahuassa *et al.* (Lahouassa et al., 2016) used a SILAC-based approach to quantify proteomic
334 changes in cells exposed to viral particles bearing Vpr, identifying 8 proteins which were depleted by
335 at least 20%. Of these, only one, HLTF was confirmed to be a direct Vpr target by targeted
336 orthogonal approaches.

337 As expected, the lists of 'candidate' Vpr proteins, identified, but not pursued, in the above studies
338 overlaps with this work, and in some instances we have confirmed these candidates to be direct
339 targets for Vpr mediated degradation. For example, SMN1 was found to bind Vpr by Jager *et al*, and
340 to be degraded by Vpr by Lahuassa *et al.* in indepenedent proteomics experiments. Similarly, ESCO2
341 was found to bind Vpr by Hrecka *et al,* but the depletion was not confirmed by immunoblot – most
342 likely due to poor performance of the commercial antibody used. We have shown here that both of
343 these proteins are direct targets for Vpr-mediated degradation.

344 By contrast to previous studies, rather than using a targeted approach to follow-up only a small
345 number of potential Vpr targets, we have combined complementary proteomic analyses to describe
346 (i) the global proteome remodelling caused by Vpr, and (ii) multiple direct substrates for Vpr-
347 mediated depletion. The two established criteria for Vpr targets, (binding and destabilisation) are
348 satisfied by numerous proteins identified here, including ESCO2, SMN1, BBX and KIF18A. These
349 proteins are therefore not candidate Vpr targets, but *bone fide* Vpr targets, proven to the same
350 standard of evidence as other, previously described substrates.

351 However, in our proposed model, Vpr binds and degrades multiple cellular proteins, with the total
352 pool of Vpr shared over multiple targets. The identification of cellular targets by co-IP is thus
353 technically problematic and more prone to false negatives compared to other proteins that establish
354 interactions with a small number of binding partners. We therefore used an alternative method of
355 identifying direct targets for Vpr mediated depletion – proteins that are post-translationally
356 degraded within 6 hours of treatment with Vpr. This strategy was more successful at capturing the
357 known effects on cellular Vpr targets than the MS-IP approach, with the degradation of HLTF and
358 ZGPAT being demonstrated within 6 hours of Vpr exposure. We are confident that the other proteins
359 identified in this fashion also represent direct targets for Vpr mediated degradation, as secondary
360 effects are excluded by both intrinsic elements of the technique, and the short time frame allowed.

361 A comparison of this work with the recent publication by Lapek *et al.* (Lapek et al., 2017) is required,
362 given similarities in approach. Lapek *et al.* used an inducible HIV-1 provirus and quantify changes to
363 the cellular proteome up to 24 hours post activation. They compared a wild type and a Vpr-deficient
364 provirus, but find many fewer differences than in this study – indeed, they identified only nine
365 proteins with significant difference between wild type and ΔVpr, none of which are previously
366 defined Vpr targets – although DCAF1 is significantly reduced in the presence of Vpr. The difference
367 most likely relates to differences between the systems used. In our model system, as in physiological
368 conditions, Vpr is delivered with the virus particle at '0 h' but de novo production of Vpr occurs late
369 in the virus lifecycle. In Lapek *et al*, the experiment is concluded 24 hours after induction of the
370 provirus. As production of de novo Vpr is Rev-dependent, Vpr production must occur after a
371 significant delay within that 24-hour period. Thus, while some limited primary effects are evident,
372 such as the depletion of DCAF1, other primary and secondary effects may not have had time to
373 occur. Aside from the matter of timing, it is also worth noting that that in the Lapek *et al.* system, all

374 Vpr is produced concurrently with Gag. The interaction between Vpr and Gag, and the recruitment
375 of a proportion of Vpr into nascent viral particles, may inhibit nuclear localisation and substrate
376 degradation.

377 Despite the importance of Vpr *in vivo*, an *in vitro* viral replication phenotype is often absent in T-cell
378 infection models (Guenzel et al., 2014). Nonetheless, expression of Vpr in T-cells causes cell cycle
379 arrest (Bolton and Lenardo, 2007; Gummuluru and Emerman, 1999; Rogel et al., 1995), cell death
380 (Bolton and Lenardo, 2007), transactivation of the viral LTR (Gummuluru and Emerman, 1999),
381 enhancement or antagonism of crucial signalling pathways including NFAT (Hohne et al., 2016) and
382 NF-κB (Liang et al., 2015; Liu et al., 2014; Muthumani et al., 2006), disruption of PARP1 localisation
383 (Hohne et al., 2016; Muthumani et al., 2006), defects in chromatid cohesion (Shimura et al., 2011)
384 and induction of the DNA damage response (Richard et al., 2010; Vassena et al., 2013). At least some
385 of these phenotypes can be segregated (Bolton and Lenardo, 2007; Hohne et al., 2016). The
386 molecular mechanisms underpinning these phenomena have remained controversial. In our model,
387 we propose that these multiple phenotypes can be explained by Vpr targeting multiple cellular
388 proteins and pathways, with potential for redundant or cumulative effects.

389 Here, we have considered the most well described cellular phenotype for Vpr, G2/M cell cycle arrest,
390 with findings compatible with this model. In addition to confirming the previously described effect of
391 Vpr mediated MCM10 degradation, we have identified three other proteins that are directly
392 targeted by Vpr, show depletion correlating with the extent of G2/M mediated arrest in a panel of
393 Vpr mutants and result in arrest at G2/M when depleted through RNAi. Notably, depletion of two of
394 these proteins, SMN1 and CDCA2 (Repo-Man), has been shown to activate the DNA damage
395 response and stimulate ATM/ATR kinase activity (Kannan et al., 2018; Peng et al., 2010),
396 demonstrated by many groups to be a critical step towards the G2/M arrest caused by Vpr (Berger et
397 al., 2015; Fregoso and Emerman, 2016; Roshal et al., 2003). The contribution of multiple Vpr targets
398 towards the same cellular phenotype may also be exemplified by another described cellular
399 phenotype for Vpr, premature chromatid segregation (PCS) (Shimura et al., 2011). While not
400 specifically investigated here, RNAi-mediated knockdown of three proteins depleted by Vpr, ESCO2,
401 CDCA5 (Sororin) and HASPIN, have been previously associated with this phenotype in different
402 systems (Dai et al., 2006; Hou and Zou, 2005; Rankin et al., 2005).

403 In conclusion, Vpr degrades multiple cellular targets, resulting in global remodelling of the host
404 proteome, and labyrinthine changes to different cellular pathways. This explains why its effects on
405 cellular phenotypes and viral replication are complex and remain poorly understood, why the
406 functional consequences of individual Vpr targets identified and studied in isolation have proved
407 elusive, and why the search for a single, critical Vpr target has been problematic.

408 **Acknowledgements**

409 This work was supported by the Wellcome Trust (PRF 101835/Z/13/Z to PJL), the MRC (CSF
410 MR/P008801/1 to NJM), NHSBT (WPA15-02 to NJM), the NIHR Cambridge BRC, and a Wellcome
411 Trust Strategic Award to the CIMR. The authors thank Dr. Reiner Schulte and the CIMR Flow
412 Cytometry Core Facility team, and the Lehner laboratory for critical discussion.

413 ## Data availability

414 In addition to **Figure 1—source data 1**, which includes data from all of the proteomics experiments
415 carried out here, proteomics data have been deposited to the ProteomeXchange Consortium via the
416 PRIDE (Vizcaino et al., 2016) partner repository with the dataset identifier PXD01029.

417 ## Experimental Procedures

418 **NL4-3 molecular clones**

419 pNL4-3-dE-EGFP (derived from the HIV-1 molecular clone pNL4-3 but encoding Enhanced Green
420 Fluorescent Protein (EGFP) in the *env* open reading frame (ORF), rendering Env non-functional) was
421 obtained through the AIDS Reagent Program, Division of AIDS, NIAD, NIH: Drs Haili Zhang, Yan Zhou,
422 and Robert Siliciano (Zhang et al., 2004) and the complete sequence verified by Sanger sequencing.
423 The ΔVpr mutant was generated by cloning three stop codons into the Vpr open reading frame,
424 immediately after the overlap with Vif to prevent interference with that gene:
425 WT Vpr ORF sequence
426 ATGGAACAAGCCCCAGAAGACCAAGGGCCACAGAGGGAGCCATACAATGAATGGACACTAGAGCTTTTAGAGGAA
427 ΔVpr ORF sequence
428 ATGGAACAAGCCCCAGAAGACCAAGGGCCACAGAGGGAGCCATACAATGAATGGACACTAGAGCTTTAATAGTAA

429 **Viral stocks**

430 VSVg-pseudotyped NL4-3-dE-EGFP HIV viral stocks were generated by co-transfection with pMD.G
431 (VSVg) as previously described (Greenwood et al., 2016). NL4-3-dE-EGFP HIV viral stocks were titred
432 by infection/transduction of known numbers of relevant target cells under standard experimental
433 conditions followed by flow cytometry for GFP and CD4 at 48 hr to identify % infected cells.
434 Single Vpr and Vpx proteins were expressed in a modified dual promotor pHRSIN (van den Boomen
435 et al., 2014) vector in which Vpr or Vpx expression is driven by the rous sarcoma virus (RSV)
436 promotor, and Emerald GFP expression is driven by the ubiquitin promotor. Virus was generated by
437 co-transfection with p8.91 and pMD.G in 293T as previously described (Greenwood et al., 2016).
438 Infectious MOI was normalised by infection in the absence of reverse transcription (RTi) inhibitors,
439 which were included where specified (see below). The panel of Vpr and Vpr proteins used are
440 detailed in **Table 2**. Amino acid sequences were codon optimized and synthesized as double
441 stranded DNA (IDT), inserted into the empty vector construct by Gibson assembly, and confirmed by
442 sanger sequencing.

443 **CEM-T4 T-cell infections**

444 CEM-T4 T-cells were infected with concentrated NL4-3-dE-EGFP or pHRSIN lentiviral stocks by
445 spinoculation at 800 ×g for 1 h in a non-refrigerated benchtop centrifuge in complete media
446 supplemented with 10 mM HEPES. Where reverse transcription treatment was specified (RTi), cells
447 were incubated with zidovudine (10 µM) and efavirenz (100 nM) (AIDS Reagent Program, Division of
448 AIDS, NIAD, NIH) for 1 hr prior to spinoculation, and inhibitors maintained at these concentrations
449 during subsequent cell culture. For MS experiments, cells were subject to dead cell removal
450 (magnetic dead cell removal kit, Miltenyi). Subsequent sample preparation, TMT labelling, and MS
451 are described below, at the end of this section.

452 **Antibodies**

453 Antibodies against the following proteins were used for immunoblot, listed by manufacturer: Atlas
454 antibodies: TASOR (HPA006735). Bethyl: BBX (A303-151A), HLTF (A300-230A), RALY (A302-070A),
455 ZNF512B (A303-234A). Cell signalling : SMN1/2 (2F1). Novus: ESCO2 (NB100-87021). Origine: UNG2
456 (2C12). Proteintech: Vpr (51143-I-AP). Santa Cruz: CCNB1 (SC-245), ZGPAT (SC-51524). Sigma: β-actin
457 (AC74). Abcam : p24 (ab9071), VCP (ab11433). The following secondary antibodies were used: goat
458 anti-mouse-HRP and anti-rabbit-HRP (immunoblot, Jackson ImmunoResearch, West Grove, PA). Anti-
459 CD4-AF647 (clone OKT4; BioLegend) and anti-CD271 (NGFR)-APC (clone ME20.4, Biolegend) were
460 used for flow cytometry.

461 **Statistical analysis**

462 Anova and Fisher's exact test analysis were carried out as described in figure legends using
463 Graphpad Prism (v7.04). TMT multiplexed proteomics datasets were analysed using a moderated T-
464 test analysis with Benjamini-Hochberg correction (Schwammle et al., 2013), carried out using R
465 (v3.3.1) (R Core Team, 2013). Significance B values for pulsed-SILAC analysis were calculated using
466 Perseus (Tyanova et al., 2016).
467
468 Further details can be found in the supplemental experimental procedures.

469 ## References

470 Ayyavoo, V., Mahboubi, A., Mahalingam, S., Ramalingam, R., Kudchodkar, S., Williams, W.V., Green,
471 D.R., and Weiner, D.B. (1997). HIV-1 Vpr suppresses immune activation and apoptosis through
472 regulation of nuclear factor kappa B. Nat Med *3*, 1117-1123.
473 Belzile, J.P., Richard, J., Rougeau, N., Xiao, Y., and Cohen, E.A. (2010). HIV-1 Vpr induces the K48-
474 linked polyubiquitination and proteasomal degradation of target cellular proteins to activate ATR
475 and promote G2 arrest. Journal of virology *84*, 3320-3330.
476 Berger, G., Lawrence, M., Hue, S., and Neil, S.J. (2015). G2/M cell cycle arrest correlates with primate
477 lentiviral Vpr interaction with the SLX4 complex. Journal of virology *89*, 230-240.
478 Boisvert, F.M., Ahmad, Y., Gierlinski, M., Charriere, F., Lamont, D., Scott, M., Barton, G., and Lamond,
479 A.I. (2012). A quantitative spatial proteomics analysis of proteome turnover in human cells. Mol Cell
480 Proteomics *11*, M111 011429.
481 Bolton, D.L., and Lenardo, M.J. (2007). Vpr cytopathicity independent of G2/M cell cycle arrest in
482 human immunodeficiency virus type 1-infected CD4+ T cells. Journal of virology *81*, 8878-8890.
483 Chougui, G., Munir-Matloob, S., Matkovic, R., Martin, M.M., Morel, M., Lahouassa, H., Leduc, M.,
484 Ramirez, B.C., Etienne, L., and Margottin-Goguet, F. (2018). HIV-2/SIV viral protein X counteracts
485 HUSH repressor complex. Nat Microbiol.
486 Coyaud, E., Ranadheera, C., Cheng, D., Goncalves, J., Dyakov, B.J.A., Laurent, E.M.N., St-Germain, J.,
487 Pelletier, L., Gingras, A.C., Brumell, J.H.*, et al.* (2018). Global Interactomics Uncovers Extensive
488 Organellar Targeting by Zika Virus. Mol Cell Proteomics *17*, 2242-2255.
489 Dai, J., Sullivan, B.A., and Higgins, J.M. (2006). Regulation of mitotic chromosome cohesion by Haspin
490 and Aurora B. Dev Cell *11*, 741-750.
491 Dehart, J.L., and Planelles, V. (2008). Human immunodeficiency virus type 1 Vpr links proteasomal
492 degradation and checkpoint activation. Journal of virology *82*, 1066-1072.
493 Diamond, D.L., Syder, A.J., Jacobs, J.M., Sorensen, C.M., Walters, K.A., Proll, S.C., McDermott, J.E.,
494 Gritsenko, M.A., Zhang, Q., Zhao, R.*, et al.* (2010). Temporal proteome and lipidome profiles reveal
495 hepatitis C virus-associated reprogramming of hepatocellular metabolism and bioenergetics. PLoS
496 Pathog *6*, e1000719.

Ersing, I., Nobre, L., Wang, L.W., Soday, L., Ma, Y., Paulo, J.A., Narita, Y., Ashbaugh, C.W., Jiang, C., Grayson, N.E.*, et al.* (2017). A Temporal Proteomic Map of Epstein-Barr Virus Lytic Replication in B Cells. Cell Rep *19*, 1479-1493.

Felzien, L.K., Woffendin, C., Hottiger, M.O., Subbramanian, R.A., Cohen, E.A., and Nabel, G.J. (1998). HIV transcriptional activation by the accessory protein, VPR, is mediated by the p300 co-activator. Proceedings of the National Academy of Sciences of the United States of America *95*, 5281-5286.

Fischer, M., Grossmann, P., Padi, M., and DeCaprio, J.A. (2016). Integration of TP53, DREAM, MMB-FOXM1 and RB-E2F target gene analyses identifies cell cycle gene regulatory networks. Nucleic Acids Res *44*, 6070-6086.

Fletcher, T.M., 3rd, Brichacek, B., Sharova, N., Newman, M.A., Stivahtis, G., Sharp, P.M., Emerman, M., Hahn, B.H., and Stevenson, M. (1996). Nuclear import and cell cycle arrest functions of the HIV-1 Vpr protein are encoded by two separate genes in HIV-2/SIV(SM). EMBO J *15*, 6155-6165.

Forget, J., Yao, X.J., Mercier, J., and Cohen, E.A. (1998). Human immunodeficiency virus type 1 vpr protein transactivation function: mechanism and identification of domains involved. J Mol Biol *284*, 915-923.

Fregoso, O.I., and Emerman, M. (2016). Activation of the DNA Damage Response Is a Conserved Function of HIV-1 and HIV-2 Vpr That Is Independent of SLX4 Recruitment. MBio *7*.

Goh, W.C., Rogel, M.E., Kinsey, C.M., Michael, S.F., Fultz, P.N., Nowak, M.A., Hahn, B.H., and Emerman, M. (1998). HIV-1 Vpr increases viral expression by manipulation of the cell cycle: a mechanism for selection of Vpr in vivo. Nat Med *4*, 65-71.

Greenwood, E.J., Matheson, N.J., Wals, K., van den Boomen, D.J., Antrobus, R., Williamson, J.C., and Lehner, P.J. (2016). Temporal proteomic analysis of HIV infection reveals remodelling of the host phosphoproteome by lentiviral Vif variants. eLife *5*.

Greenwood, E.J., Schmidt, F., Kondova, I., Niphuis, H., Hodara, V.L., Clissold, L., McLay, K., Guerra, B., Redrobe, S., Giavedoni, L.D.*, et al.* (2015). Simian Immunodeficiency Virus Infection of Chimpanzees (Pan troglodytes) Shares Features of Both Pathogenic and Non-pathogenic Lentiviral Infections. PLoS Pathog *11*, e1005146.

Guenzel, C.A., Herate, C., and Benichou, S. (2014). HIV-1 Vpr-a still "enigmatic multitasker". Front Microbiol *5*, 127.

Gummuluru, S., and Emerman, M. (1999). Cell cycle- and Vpr-mediated regulation of human immunodeficiency virus type 1 expression in primary and transformed T-cell lines. Journal of virology *73*, 5422-5430.

Guo, Z., Kong, Q., Liu, C., Zhang, S., Zou, L., Yan, F., Whitmire, J.K., Xiong, Y., Chen, X., and Wan, Y.Y. (2016). DCAF1 controls T-cell function via p53-dependent and -independent mechanisms. Nat Commun *7*, 10307.

Hofmann, S., Dehn, S., Businger, R., Bolduan, S., Schneider, M., Debyser, Z., Brack-Werner, R., and Schindler, M. (2017). Dual role of the chromatin-binding factor PHF13 in the pre- and post-integration phases of HIV-1 replication. Open biology *7*.

Hohne, K., Businger, R., van Nuffel, A., Bolduan, S., Koppensteiner, H., Baeyens, A., Vermeire, J., Malatinkova, E., Verhasselt, B., and Schindler, M. (2016). Virion encapsidated HIV-1 Vpr induces NFAT to prime non-activated T cells for productive infection. Open Biol *6*.

Hossain, D., Javadi Esfehani, Y., Das, A., and Tsang, W.Y. (2017). Cep78 controls centrosome homeostasis by inhibiting EDD-DYRK2-DDB1(Vpr)(BP). EMBO Rep *18*, 632-644.

Hou, F., and Zou, H. (2005). Two human orthologues of Eco1/Ctf7 acetyltransferases are both required for proper sister-chromatid cohesion. Mol Biol Cell *16*, 3908-3918.

Hrecka, K., Hao, C., Gierszewska, M., Swanson, S.K., Kesik-Brodacka, M., Srivastava, S., Florens, L., Washburn, M.P., and Skowronski, J. (2011). Vpx relieves inhibition of HIV-1 infection of macrophages mediated by the SAMHD1 protein. Nature *474*, 658-661.

Hrecka, K., Hao, C., Shun, M.C., Kaur, S., Swanson, S.K., Florens, L., Washburn, M.P., and Skowronski, J. (2016). HIV-1 and HIV-2 exhibit divergent interactions with HLTF and UNG2 DNA repair proteins. Proceedings of the National Academy of Sciences of the United States of America *113*, E3921-3930.

548 Jager, S., Cimermancic, P., Gulbahce, N., Johnson, J.R., McGovern, K.E., Clarke, S.C., Shales, M.,
549 Mercenne, G., Pache, L., Li, K.*, et al.* (2011). Global landscape of HIV-human protein complexes.
550 Nature *481*, 365-370.
551 Kannan, A., Bhatia, K., Branzei, D., and Gangwani, L. (2018). Combined deficiency of Senataxin and
552 DNA-PKcs causes DNA damage accumulation and neurodegeneration in spinal muscular atrophy.
553 Nucleic Acids Res *46*, 8326-8346.
554 Keele, B.F., Jones, J.H., Terio, K.A., Estes, J.D., Rudicell, R.S., Wilson, M.L., Li, Y., Learn, G.H., Beasley,
555 T.M., Schumacher-Stankey, J.*, et al.* (2009). Increased mortality and AIDS-like immunopathology in
556 wild chimpanzees infected with SIVcpz. Nature *460*, 515-519.
557 Laguette, N., Bregnard, C., Hue, P., Basbous, J., Yatim, A., Larroque, M., Kirchhoff, F., Constantinou,
558 A., Sobhian, B., and Benkirane, M. (2014). Premature activation of the SLX4 complex by Vpr
559 promotes G2/M arrest and escape from innate immune sensing. Cell *156*, 134-145.
560 Laguette, N., Sobhian, B., Casartelli, N., Ringeard, M., Chable-Bessia, C., Segeral, E., Yatim, A.,
561 Emiliani, S., Schwartz, O., and Benkirane, M. (2011). SAMHD1 is the dendritic- and myeloid-cell-
562 specific HIV-1 restriction factor counteracted by Vpx. Nature *474*, 654-657.
563 Lahouassa, H., Blondot, M.L., Chauveau, L., Chougui, G., Morel, M., Leduc, M., Guillonneau, F.,
564 Ramirez, B.C., Schwartz, O., and Margottin-Goguet, F. (2016). HIV-1 Vpr degrades the HLTF DNA
565 translocase in T cells and macrophages. Proceedings of the National Academy of Sciences of the
566 United States of America.
567 Lahti, A.L., Manninen, A., and Saksela, K. (2003). Regulation of T cell activation by HIV-1 accessory
568 proteins: Vpr acts via distinct mechanisms to cooperate with Nef in NFAT-directed gene expression
569 and to promote transactivation by CREB. Virology *310*, 190-196.
570 Lapek, J.D., Jr., Lewinski, M.K., Wozniak, J.M., Guatelli, J., and Gonzalez, D.J. (2017). Quantitative
571 Temporal Viromics of an Inducible HIV-1 Model Yields Insight to Global Host Targets and Phospho-
572 Dynamics Associated with Protein Vpr. Mol Cell Proteomics *16*, 1447-1461.
573 Le Rouzic, E., Belaidouni, N., Estrabaud, E., Morel, M., Rain, J.C., Transy, C., and Margottin-Goguet, F.
574 (2007). HIV1 Vpr arrests the cell cycle by recruiting DCAF1/VprBP, a receptor of the Cul4-DDB1
575 ubiquitin ligase. Cell Cycle *6*, 182-188.
576 Liang, Z., Liu, R., Lin, Y., Liang, C., Tan, J., and Qiao, W. (2015). HIV-1 Vpr protein activates the NF-
577 kappaB pathway to promote G2/M cell cycle arrest. Virol Sin *30*, 441-448.
578 Lim, E.S., Fregoso, O.I., McCoy, C.O., Matsen, F.A., Malik, H.S., and Emerman, M. (2012). The ability
579 of primate lentiviruses to degrade the monocyte restriction factor SAMHD1 preceded the birth of
580 the viral accessory protein Vpx. Cell host & microbe *11*, 194-204.
581 Liu, R., Lin, Y., Jia, R., Geng, Y., Liang, C., Tan, J., and Qiao, W. (2014). HIV-1 Vpr stimulates NF-kappaB
582 and AP-1 signaling by activating TAK1. Retrovirology *11*, 45.
583 Luo, Y., Jacobs, E.Y., Greco, T.M., Mohammed, K.D., Tong, T., Keegan, S., Binley, J.M., Cristea, I.M.,
584 Fenyo, D., Rout, M.P.*, et al.* (2016). HIV-host interactome revealed directly from infected cells. Nat
585 Microbiol *1*, 16068.
586 Lv, L., Wang, Q., Xu, Y., Tsao, L.C., Nakagawa, T., Guo, H., Su, L., and Xiong, Y. (2018). Vpr Targets
587 TET2 for Degradation by CRL4(VprBP) E3 Ligase to Sustain IL-6 Expression and Enhance HIV-1
588 Replication. Mol Cell *70*, 961-970 e965.
589 Ly, T., Endo, A., and Lamond, A.I. (2015). Proteomic analysis of the response to cell cycle arrests in
590 human myeloid leukemia cells. eLife *4*.
591 Matheson, N.J., Greenwood, E.J., and Lehner, P.J. (2016). Manipulation of immunometabolism by
592 HIV-accessories to the crime? Curr Opin Virol *19*, 65-70.
593 Matheson, N.J., Sumner, J., Wals, K., Rapiteanu, R., Weekes, M.P., Vigan, R., Weinelt, J., Schindler,
594 M., Antrobus, R., Costa, A.S.*, et al.* (2015). Cell Surface Proteomic Map of HIV Infection Reveals
595 Antagonism of Amino Acid Metabolism by Vpu and Nef. Cell host & microbe *18*, 409-423.
596 Maudet, C., Sourisce, A., Dragin, L., Lahouassa, H., Rain, J.C., Bouaziz, S., Ramirez, B.C., and
597 Margottin-Goguet, F. (2013). HIV-1 Vpr induces the degradation of ZIP and sZIP, adaptors of the
598 NuRD chromatin remodeling complex, by hijacking DCAF1/VprBP. PLoS One *8*, e77320.

Murray, J.M., Kelleher, A.D., and Cooper, D.A. (2011). Timing of the components of the HIV life cycle in productively infected CD4+ T cells in a population of HIV-infected individuals. Journal of virology *85*, 10798-10805.
Muthumani, K., Choo, A.Y., Zong, W.X., Madesh, M., Hwang, D.S., Premkumar, A., Thieu, K.P., Emmanuel, J., Kumar, S., Thompson, C.B.*, et al.* (2006). The HIV-1 Vpr and glucocorticoid receptor complex is a gain-of-function interaction that prevents the nuclear localization of PARP-1. Nat Cell Biol *8*, 170-179.
Naamati, A., Williamson, J.C., Greenwood, E.J., Marelli, S., Lehner, P.J., and Matheson, N.J. (2018). Functional proteomic atlas of HIV-infection in primary human CD4+ T cells. bioRxiv.
Peng, A., Lewellyn, A.L., Schiemann, W.P., and Maller, J.L. (2010). Repo-man controls a protein phosphatase 1-dependent threshold for DNA damage checkpoint activation. Curr Biol *20*, 387-396.
Perelson, A.S., Neumann, A.U., Markowitz, M., Leonard, J.M., and Ho, D.D. (1996). HIV-1 dynamics in vivo: virion clearance rate, infected cell life-span, and viral generation time. Science *271*, 1582-1586.
R Core Team (2013). R: A language and environment for statistical computing. Vienna, Austria http://wwwR-projectorg/.
Rankin, S., Ayad, N.G., and Kirschner, M.W. (2005). Sororin, a substrate of the anaphase-promoting complex, is required for sister chromatid cohesion in vertebrates. Mol Cell *18*, 185-200.
Re, F., Braaten, D., Franke, E.K., and Luban, J. (1995). Human immunodeficiency virus type 1 Vpr arrests the cell cycle in G2 by inhibiting the activation of p34cdc2-cyclin B. Journal of virology *69*, 6859-6864.
Richard, J., Sindhu, S., Pham, T.N., Belzile, J.P., and Cohen, E.A. (2010). HIV-1 Vpr up-regulates expression of ligands for the activating NKG2D receptor and promotes NK cell-mediated killing. Blood *115*, 1354-1363.
Rogel, M.E., Wu, L.I., and Emerman, M. (1995). The human immunodeficiency virus type 1 vpr gene prevents cell proliferation during chronic infection. Journal of virology *69*, 882-888.
Romani, B., Shaykh Baygloo, N., Aghasadeghi, M.R., and Allahbakhshi, E. (2015). HIV-1 Vpr Protein Enhances Proteasomal Degradation of MCM10 DNA Replication Factor through the Cul4-DDB1[VprBP] E3 Ubiquitin Ligase to Induce G2/M Cell Cycle Arrest. J Biol Chem *290*, 17380-17389.
Roshal, M., Kim, B., Zhu, Y., Nghiem, P., and Planelles, V. (2003). Activation of the ATR-mediated DNA damage response by the HIV-1 viral protein R. J Biol Chem *278*, 25879-25886.
Roux, P., Alfieri, C., Hrimech, M., Cohen, E.A., and Tanner, J.E. (2000). Activation of transcription factors NF-kappaB and NF-IL-6 by human immunodeficiency virus type 1 protein R (Vpr) induces interleukin-8 expression. Journal of virology *74*, 4658-4665.
Schrofelbauer, B., Yu, Q., Zeitlin, S.G., and Landau, N.R. (2005). Human immunodeficiency virus type 1 Vpr induces the degradation of the UNG and SMUG uracil-DNA glycosylases. Journal of virology *79*, 10978-10987.
Schwammle, V., Leon, I.R., and Jensen, O.N. (2013). Assessment and improvement of statistical tools for comparative proteomics analysis of sparse data sets with few experimental replicates. Journal of proteome research *12*, 3874-3883.
Selig, L., Benichou, S., Rogel, M.E., Wu, L.I., Vodicka, M.A., Sire, J., Benarous, R., and Emerman, M. (1997). Uracil DNA glycosylase specifically interacts with Vpr of both human immunodeficiency virus type 1 and simian immunodeficiency virus of sooty mangabeys, but binding does not correlate with cell cycle arrest. Journal of virology *71*, 4842-4846.
Shimura, M., Toyoda, Y., Iijima, K., Kinomoto, M., Tokunaga, K., Yoda, K., Yanagida, M., Sata, T., and Ishizaka, Y. (2011). Epigenetic displacement of HP1 from heterochromatin by HIV-1 Vpr causes premature sister chromatid separation. J Cell Biol *194*, 721-735.
Simon, V., Bloch, N., and Landau, N.R. (2015). Intrinsic host restrictions to HIV-1 and mechanisms of viral escape. Nat Immunol *16*, 546-553.
Sugden, S.M., Bego, M.G., Pham, T.N., and Cohen, E.A. (2016). Remodeling of the Host Cell Plasma Membrane by HIV-1 Nef and Vpu: A Strategy to Ensure Viral Fitness and Persistence. Viruses *8*.

649 Sumner, R.P., Thorne, L.G., Fink, D.L., Khan, H., Milne, R.S., and Towers, G.J. (2017). Are Evolution
650 and the Intracellular Innate Immune System Key Determinants in HIV Transmission? Front Immunol
651 *8*, 1246.
652 Tchasovnikarova, I.A., Timms, R.T., Matheson, N.J., Wals, K., Antrobus, R., Gottgens, B., Dougan, G.,
653 Dawson, M.A., and Lehner, P.J. (2015). GENE SILENCING. Epigenetic silencing by the HUSH complex
654 mediates position-effect variegation in human cells. Science *348*, 1481-1485.
655 Terada, Y., and Yasuda, Y. (2006). Human immunodeficiency virus type 1 Vpr induces G2 checkpoint
656 activation by interacting with the splicing factor SAP145. Mol Cell Biol *26*, 8149-8158.
657 Tyanova, S., Temu, T., Sinitcyn, P., Carlson, A., Hein, M.Y., Geiger, T., Mann, M., and Cox, J. (2016).
658 The Perseus computational platform for comprehensive analysis of (prote)omics data. Nat Methods
659 *13*, 731-740.
660 van den Boomen, D.J., Timms, R.T., Grice, G.L., Stagg, H.R., Skodt, K., Dougan, G., Nathan, J.A., and
661 Lehner, P.J. (2014). TMEM129 is a Derlin-1 associated ERAD E3 ligase essential for virus-induced
662 degradation of MHC-I. Proceedings of the National Academy of Sciences of the United States of
663 America *111*, 11425-11430.
664 Vassena, L., Giuliani, E., Matusali, G., Cohen, E.A., and Doria, M. (2013). The human
665 immunodeficiency virus type 1 Vpr protein upregulates PVR via activation of the ATR-mediated DNA
666 damage response pathway. J Gen Virol *94*, 2664-2669.
667 Vizcaino, J.A., Csordas, A., Del-Toro, N., Dianes, J.A., Griss, J., Lavidas, I., Mayer, G., Perez-Riverol, Y.,
668 Reisinger, F., Ternent, T.*, et al.* (2016). 2016 update of the PRIDE database and its related tools.
669 Nucleic Acids Res *44*, 11033.
670 Weekes, M.P., Tomasec, P., Huttlin, E.L., Fielding, C.A., Nusinow, D., Stanton, R.J., Wang, E.C.,
671 Aicheler, R., Murrell, I., Wilkinson, G.W.*, et al.* (2014). Quantitative temporal viromics: an approach
672 to investigate host-pathogen interaction. Cell *157*, 1460-1472.
673 Wu, Y., Zhou, X., Barnes, C.O., DeLucia, M., Cohen, A.E., Gronenborn, A.M., Ahn, J., and Calero, G.
674 (2016). The DDB1-DCAF1-Vpr-UNG2 crystal structure reveals how HIV-1 Vpr steers human UNG2
675 toward destruction. Nat Struct Mol Biol *23*, 933-940.
676 Yurkovetskiy, L., Guney, M.H., Kim, K., Goh, S.L., McCauley, S., Dauphin, A., Diehl, W.E., and Luban, J.
677 (2018). Primate immunodeficiency virus proteins Vpx and Vpr counteract transcriptional repression
678 of proviruses by the HUSH complex. Nat Microbiol.
679 Zhang, H., Zhou, Y., Alcock, C., Kiefer, T., Monie, D., Siliciano, J., Li, Q., Pham, P., Cofrancesco, J.,
680 Persaud, D.*, et al.* (2004). Novel single-cell-level phenotypic assay for residual drug susceptibility and
681 reduced replication capacity of drug-resistant human immunodeficiency virus type 1. Journal of
682 virology *78*, 1718-1729.
683 Zhou, X., DeLucia, M., and Ahn, J. (2016). SLX4-SLX1 Protein-independent Down-regulation of
684 MUS81-EME1 Protein by HIV-1 Viral Protein R (Vpr). J Biol Chem *291*, 16936-16947.
685 Zhou, Y., and Ratner, L. (2000). Phosphorylation of human immunodeficiency virus type 1 Vpr
686 regulates cell cycle arrest. Journal of virology *74*, 6520-6527.

687

688 ## Figure legends

689 **Figure 1. Proteomic analysis of the effect of Vpr in HIV infection.**

690 **A**, Graphical summary of the HIV and ΔVpr HIV infection TMT experiment. Three replicates of
691 uninfected (mock), WT HIV infected and ΔVpr infected cells were prepared and analysed in parallel
692 using TMT labelling. **B,** FACS plots showing the quantification of infection in an example replicate for
693 each of the three conditions. Infected cells lose CD4 expression and become GFP positive. **C,**
694 Scatterplots displaying pairwise comparisons between WT, ΔVpr and mock-infected cells. Each point
695 represents a single protein, with HIV proteins and host proteins of interest highlighted with different

696 symbols (see key). **D,** Principle component analysis of the samples in this experiment, with WT
697 infected replicates in red, ΔVpr in blue and mock infected cells in grey.

698 **Figure 2. Analysis of the nature of Vpr mediated proteome remodelling.**

699 **A**, Graphical summary of the Vpr viral particle TMT experiment. Three replicates of cells exposed to
700 empty viral particles or Vpr bearing viral particles, along with single replicates of cells exposed to
701 viral particles bearing five different Vpr mutants were prepared and analysed in parallel using TMT
702 labelling. **B,** Scatterplot displaying pairwise comparison between cells exposed to empty or Vpr
703 bearing viral particles. **C**, Scatterplot comparing pairwise comparisons from two proteomics
704 experiments, demonstrating the effect of Vpr in the context of HIV-1 infection (x-axis, as shown in
705 **Figure 1A**) or through cellular exposure to Vpr protein alone (y- axis, as shown in **Figure 2A**). **D**,
706 scatterplots showing the pairwise comparison between each Vpr mutant tested and empty vector
707 control, with defined groups of 302 Vpr depleted and 413 increased proteins highlighted in blue and
708 red respectively. **E**, Defined groups of Vpr depleted and increased proteins were subject to gene
709 ontology enrichment analysis, compared with a background of all proteins quantitated in these
710 experiments. GO Cellular compartment enrichment analysis results were manually curated for 9
711 commonly used organelle level classifications, shown here. + / - indicates if the classification was
712 enriched or de-enriched compared with the expected number of proteins expected by chance.
713 Where significant, associated p value represents the results of a Fisher's exact test with Bonferroni
714 correction. This is highly conservative as it is corrected for all 1061 possible cellular compartment
715 terms, not just those shown.

716 **Figure 3. Pulsed SILAC method to identify direct targets for Vpr mediated decay.**

717 **A,** Graphical summary of the pulsed SILAC experiment. **B,** Scatterplots showing the changes to
718 protein stability of proteins after 6 or 24 hours of exposure to Vpr bearing lentivirus compared to
719 control lentivirus, with defined groups of 302 Vpr depleted (blue) and 413 increased (red) proteins
720 highlighted. **C,** Expanded view of proteins degraded within 6 hours of Vpr exposure. Significantly
721 degraded (Sig.B <0.01) proteins are highlighted in gold. Previously described Vpr targets HLTF,
722 MUS81 and ZGPAT are shown in purple. **D,** Graphical summary of the direct targets for Vpr mediated
723 degradation. Proteins highlighted in purple are previously described Vpr targets, proteins with red
724 text were predicted as potential Vpr targets based on their temporal profile of depletion in
725 Greenwood & Matheson, 2016 (Greenwood et al., 2016).

726 **Figure 4. Novel Vpr targets involved in G2/M arrest.**

727 **A,** Correlation between depletion of MCM10, MUS81 and EME1 by each Vpr mutant tested in the
728 experiment shown in **Figure 2** and the extent of G2/M arrest caused by that mutant. Red line shows
729 linear regression analysis. **B,** Example DNA staining showing G2/M arrest caused by shRNA mediated
730 depletion of MCM10, representative of three independent experiments. Watson pragmatic
731 modelling was used to identify cells in G1 (blue), S (grey) or G2/M (red) phase. **C**, Real-time qRT-PCR
732 analysis of MCM10 mRNA abundance in cells transduced with control or MCM10 targeting shRNA.
733 Values were generated using the ΔΔCT method, relative to GAPDH mRNA abundance and normalised
734 to the control condition. Bars show mean values, error bars show SEM of three technical replicates.
735 **D,** Targeted shRNA screen of direct Vpr target proteins identified here, whose depletion correlated
736 with G2/M arrest in **Figure 2.** Bars show averages of at least two replicates from more than three
737 independent experiments, error bars showing SEM. Dashed lines show control average +/- 3

standard deviations. Control condition contains combined data from three different control shRNA. **B,** Real-time qRT-PCR analysis of mRNA abundance in cells transduced with control or targeting shRNA. Values were generated using the ΔΔCT method, relative to GAPDH mRNA abundance and normalised to the control condition. Bars show mean values, error bars show SEM of three technical replicates. **C,** Example DNA staining showing G2/M arrest caused by shRNA mediated depletion of SMN1, CDCA2 and ZNF267, representative of at least two independent experiments.

Figure 5. Identification of proteome changes conserved between human and primate lentiviral Vpr lineages. A, Graphical summary of the TMT experiment testing conservation of Vpr functions. **B**, Scatterplots showing the pairwise comparison between each Vpr tested and empty vector control with defined groups of 302 Vpr depleted (blue) and 413 increased (red) proteins highlighted. **C,** Bar chart showing proteins from the significantly Vpr depleted group that were profoundly (more than 50%) depleted in more than one lineage, of the four lineages tested (HIV-1/SIVcpz, HIV-2/SIVsmm, SIVagm, SIVrcm). Gold bars indicate proteins identified as direct targets for Vpr mediated degradation, DCAF1, known to interact with Vpr from multiple lineages, is highlighted in purple. **D**, Immunoblot of example known, non-conserved and conserved targets of Vpr mediated depletion. N.B. The HIV-2 Vpr is a primary isolate HIV-2 Vpr (7312a), while the proteomics experiment described in Figure 5A included HIV-2 ROD Vpr. **E**, Graphical summary of the TMT experiment to examine proteome changes in cells transduced with HIV-2 Vpr and Vpx for an extended period. **F,** Scatterplots displaying pairwise comparison between cells transduced with 7312a HIV-2 Vpr and Vpx for 96 h compared with those transduced with empty vector for 96 h. Blue and red dots represent the defined groups or proteins depleted or increased by NL4-3 Vpr respectively. Points ringed in gold indicate direct targets for NL4-3 Vpr mediated degradation listed in Table 1.

Figure 1

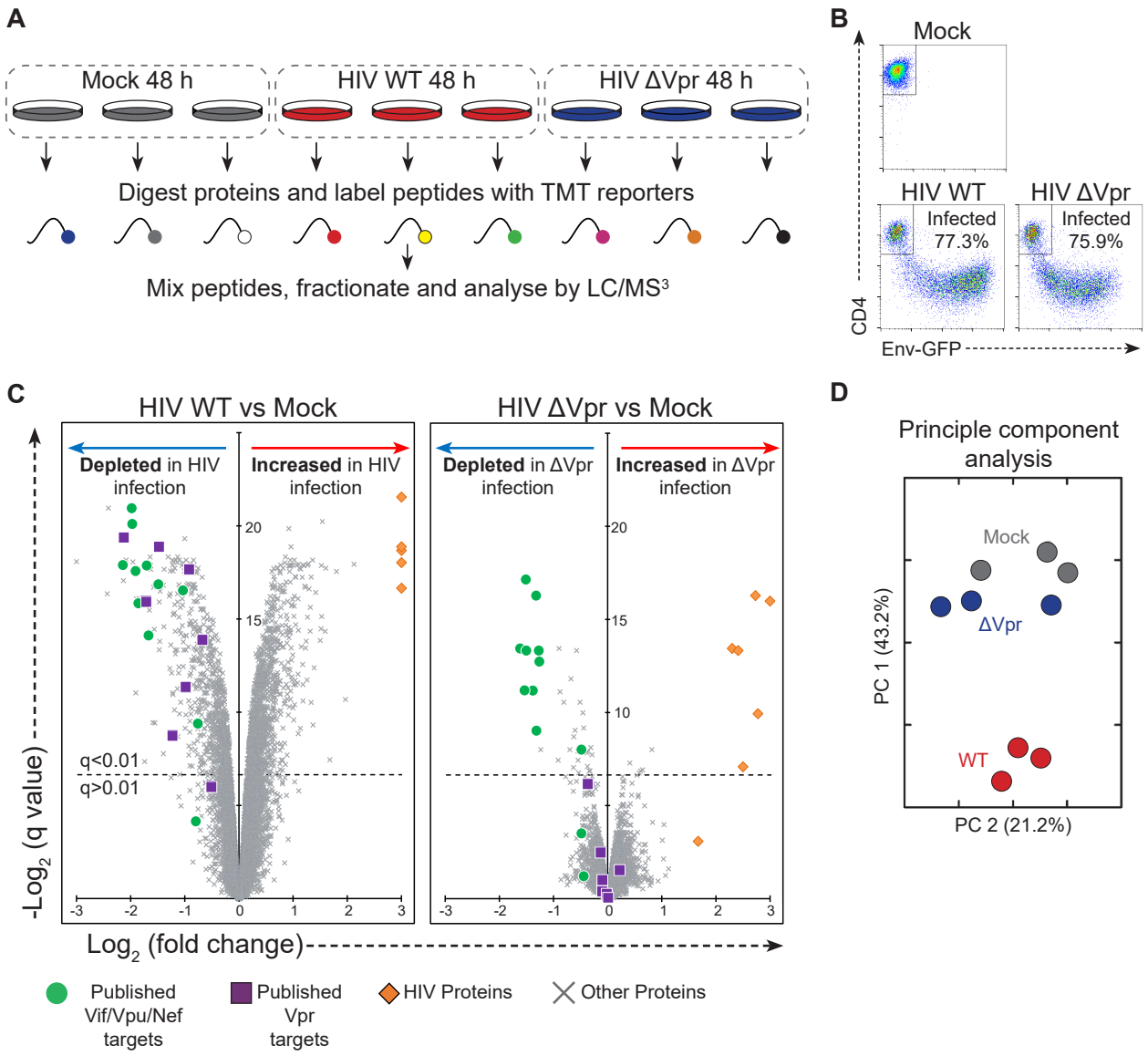
A
Mock 48 h
HIV WT 48 h
HIV ΔVpr 48 h
Digest proteins and label peptides with TMT reporters
Mix peptides, fractionate and analyse by LC/MS³
B
Mock
HIV WT
HIV ΔVpr
Infected 77.3%
Infected 75.9%
CD4
Env-GFP
C
HIV WT vs Mock
HIV ΔVpr vs Mock
Depleted in HIV infection
Increased in HIV infection
Depleted in ΔVpr infection
Increased in ΔVpr infection
q<0.01
q>0.01
-Log2 (q value)
Log2 (fold change)
Published Vif/Vpu/Nef targets
Published Vpr targets
HIV Proteins
Other Proteins
D
Principle component analysis
Mock
ΔVpr
WT
PC 1 (43.2%)
PC 2 (21.2%)

Figure 2

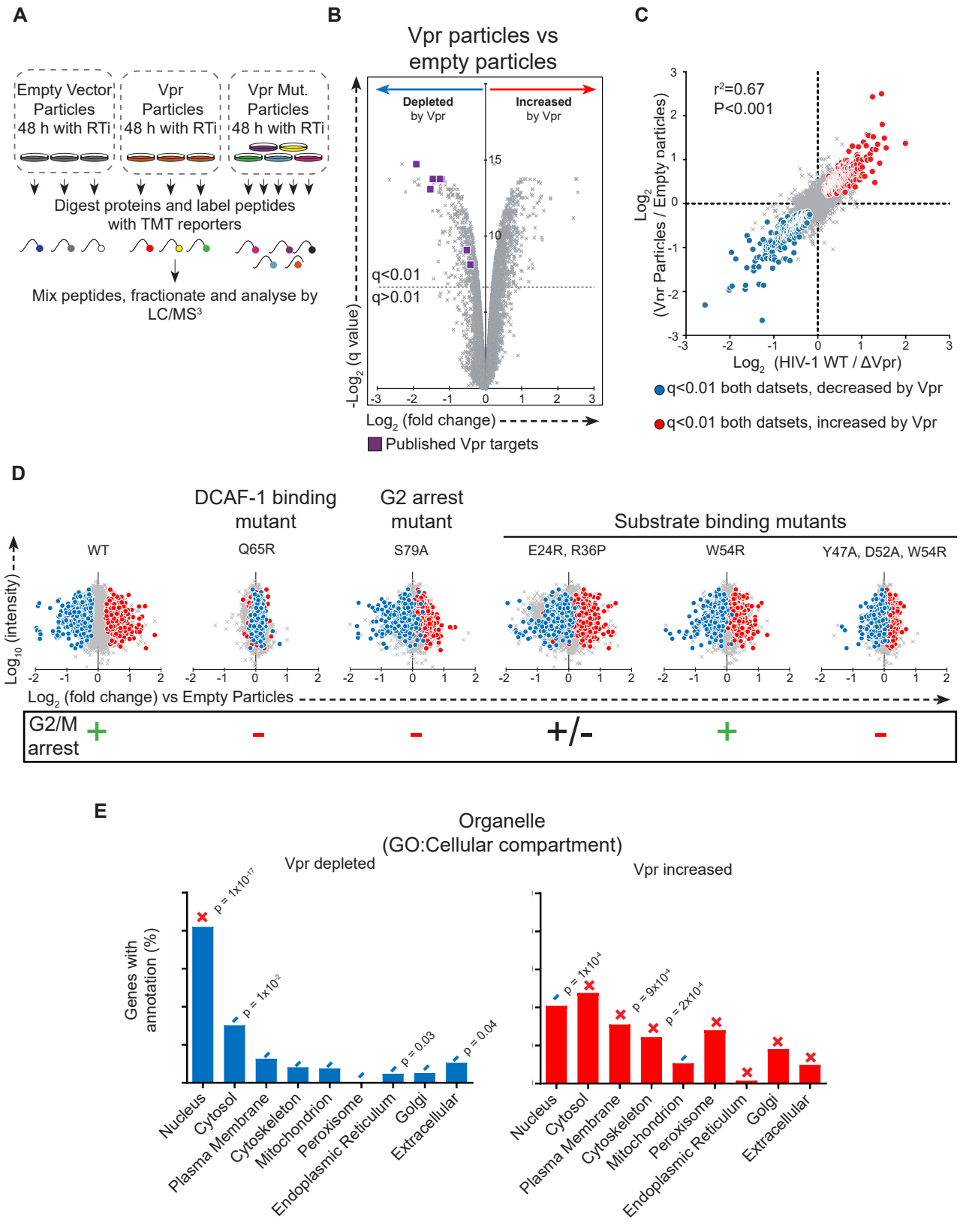
A
Empty Vector Particles 48 h with RTi
Vpr Particles 48 h with RTi
Vpr Mut. Particles 48 h with RTi
Digest proteins and label peptides with TMT reporters
Mix peptides, fractionate and analyse by LC/MS3
B
Vpr particles vs empty particles
Depleted by Vpr
Increased by Vpr
q<0.01
q>0.01
-Log2 (q value)
Log2 (fold change)
Published Vpr targets
C
r2=0.67
P<0.001
Log2 (Vpr Particles / Empty particles)
Log2 (HIV-1 WT / ΔVpr)
q<0.01 both datsets, decreased by Vpr
q<0.01 both datsets, increased by Vpr
D
DCAF-1 binding mutant
G2 arrest mutant
Substrate binding mutants
WT
Q65R
S79A
E24R, R36P
W54R
Y47A, D52A, W54R
Log10 (intensity)
Log2 (fold change) vs Empty Particles
G2/M arrest
+
-
-
+/-
+
-
E
Organelle (GO:Cellular compartment)
Vpr depleted
Vpr increased
Genes with annotation (%)
p = 1x10-17
p = 1x10-2
p = 0.03
p = 0.04
p = 1x10-4
p = 9x10-4
p = 2x10-4
Nucleus
Cytosol
Plasma Membrane
Cytoskeleton
Mitochondrion
Peroxisome
Endoplasmic Reticulum
Golgi
Extracellular

Figure 3

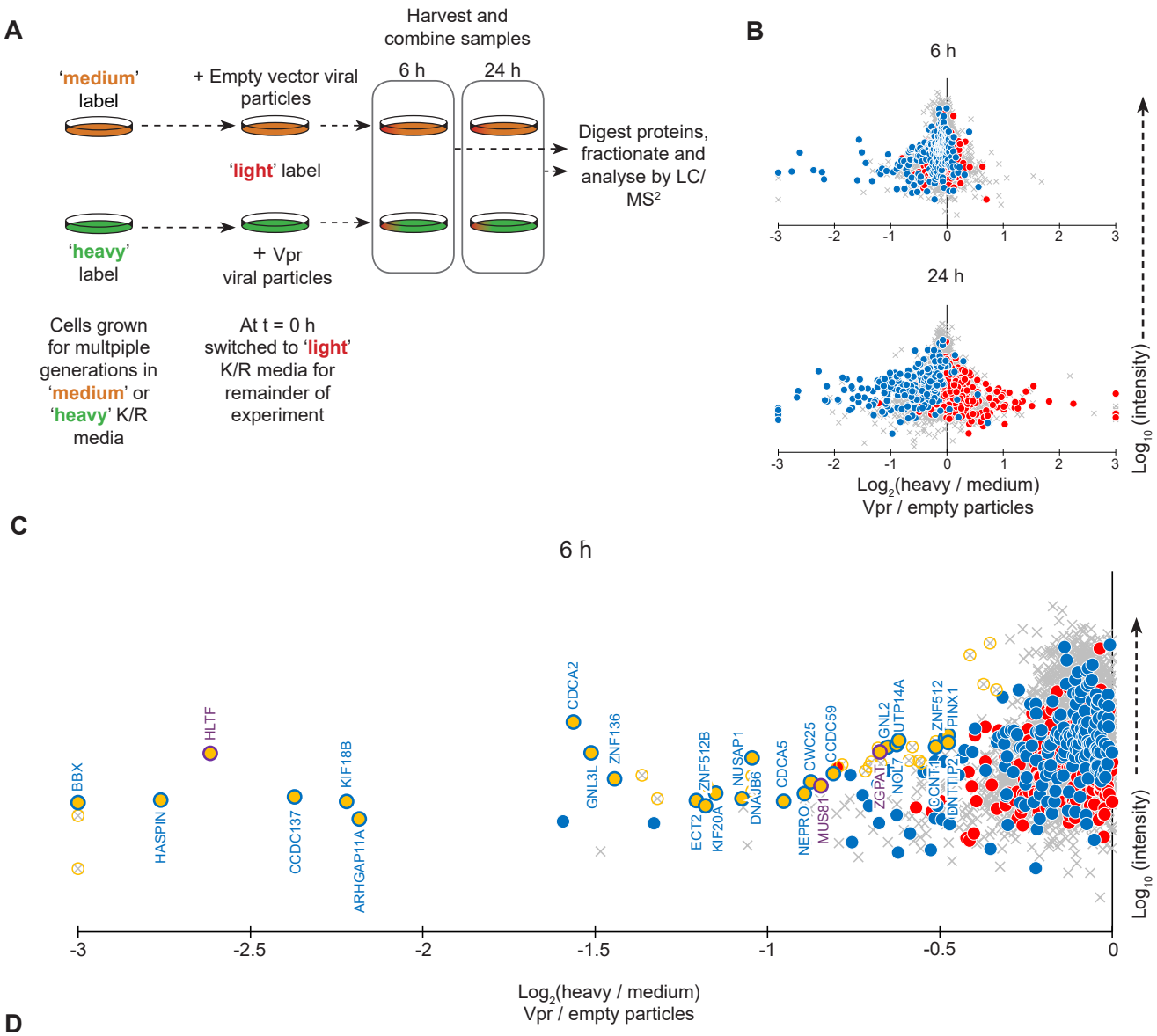

D

Accession	Gene	Vpr necessary	Incoming Vpr sufficient	Degraded within 6 h	Co-IP
Q56NI9	ESCO2	Yes	Yes	ND	Yes
Q16637	SMN1 / SMN2	Yes	Yes	NS	Yes
Q14527	HLTF	Yes	Yes	Yes	-
Q96KM6	ZNF512B	Yes	Yes	Yes	-
Q8WY36	BBX	Yes	Yes	Yes	Yes
A6NFI3	ZNF316	Yes	Yes	Yes	-
Q8NI77	KIF18A	Yes	Yes	ND	Yes
Q8TF76	HASPIN	Yes	Yes	Yes	-
Q9Y4B6	VPRBP	Yes	Yes	NS	Yes
Q96FF9	CDCA5	Yes	Yes	Yes	-
Q6PK04	CCDC137	Yes	Yes	Yes	-
Q9NXE8	CWC25	Yes	Yes	Yes	-
Q86Y91	KIF18B	Yes	Yes	Yes	-
Q6P4F7	ARHGAP11A	Yes	Yes	Yes	-
Q6NW34	NEPRO	Yes	Yes	Yes	-
Q9BVJ6	UTP14A	Yes	Yes	Yes	-
Q9NVN8	GNL3L	Yes	Yes	Yes	-
Q5QJE6	DNTTIP2	Yes	Yes	Yes	-
Q69YH5	CDCA2	Yes	Yes	Yes	-

Accession	Gene	Vpr necessary	Incoming Vpr sufficient	Degraded within 6 h	Co-IP
Q96BK5	PINX1	Yes	Yes	Yes	-
Q8N5A5	ZGPAT	Yes	Yes	Yes	-
Q13823	GNL2	Yes	Yes	Yes	-
Q9UHI6	DDX20	Yes	Yes	NS	Yes
Q96ME7	ZNF512	Yes	Yes	Yes	-
Q14586	ZNF267	Yes	Yes	NS	Yes
Q9H8V3	ECT2	Yes	Yes	Yes	-
P57678	GEMIN4	Yes	Yes	NS	Yes
P52701	MSH6	Yes	Yes	NS	Yes
O75190	DNAJB6	Yes	Yes	Yes	-
Q96NY9	MUS81	Yes	Yes	Yes	-
O60563	CCNT1	Yes	Yes	Yes	-
Q9P031	CCDC59	Yes	Yes	Yes	-
Q9UIS9	MBD1	Yes	Yes	NS	Yes
Q9UMY1	NOL7	Yes	Yes	Yes	-
Q6ZN55	ZNF574	Yes	Yes	NS	Yes
Q9BXS6	NUSAP1	Yes	Yes	Yes	-
O95235	KIF20A	Yes	Yes	Yes	-
P35251	RFC1	Yes	Yes	NS	Yes

ND: Not detected in this experiment
NS: Degraded with Sig.B >0.01

Figure 4

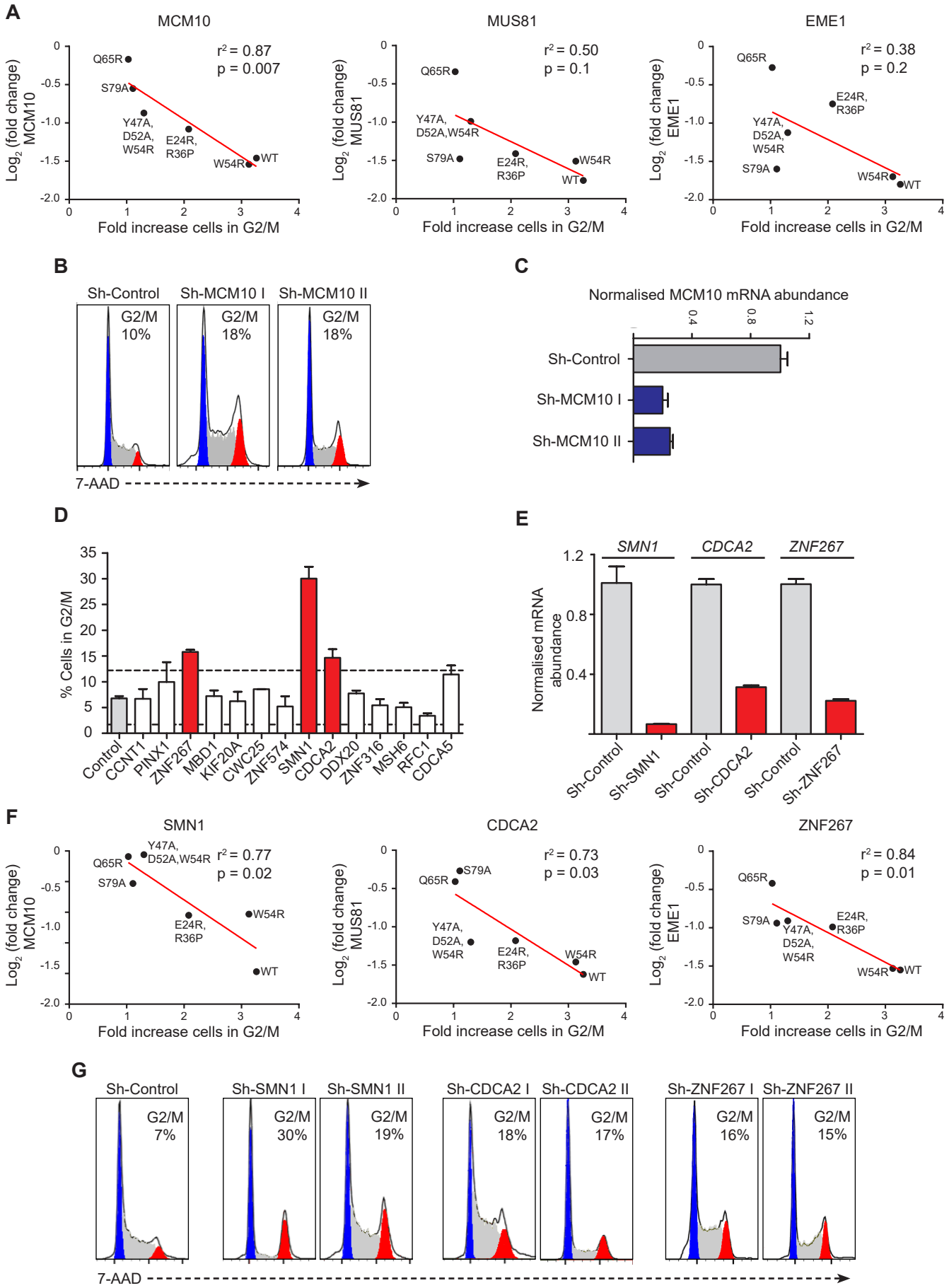
A
MCM10
MUS81
EME1
r² = 0.87
p = 0.007
r² = 0.50
p = 0.1
r² = 0.38
p = 0.2
Log₂ (fold change) MCM10
Log₂ (fold change) MUS81
Log₂ (fold change) EME1
Fold increase cells in G2/M
Q65R
S79A
Y47A, D52A, W54R
E24R, R36P
W54R
WT
Y47A, D52A,W54R
B
Sh-Control
Sh-MCM10 I
Sh-MCM10 II
G2/M 10%
G2/M 18%
G2/M 18%
7-AAD
C
Normalised MCM10 mRNA abundance
D
% Cells in G2/M
Control
CCNT1
PINX1
ZNF267
MBD1
KIF20A
CWC25
ZNF574
SMN1
CDCA2
DDX20
ZNF316
MSH6
RFC1
CDCA5
E
SMN1
CDCA2
ZNF267
Normalised mRNA abundance
Sh-Control
Sh-SMN1
Sh-CDCA2
Sh-ZNF267
F
SMN1
CDCA2
ZNF267
r² = 0.77
p = 0.02
r² = 0.73
p = 0.03
r² = 0.84
p = 0.01
G
Sh-Control
Sh-SMN1 I
Sh-SMN1 II
Sh-CDCA2 I
Sh-CDCA2 II
Sh-ZNF267 I
Sh-ZNF267 II
G2/M 7%
G2/M 30%
G2/M 19%
G2/M 18%
G2/M 17%
G2/M 16%
G2/M 15%
7-AAD

Figure 5

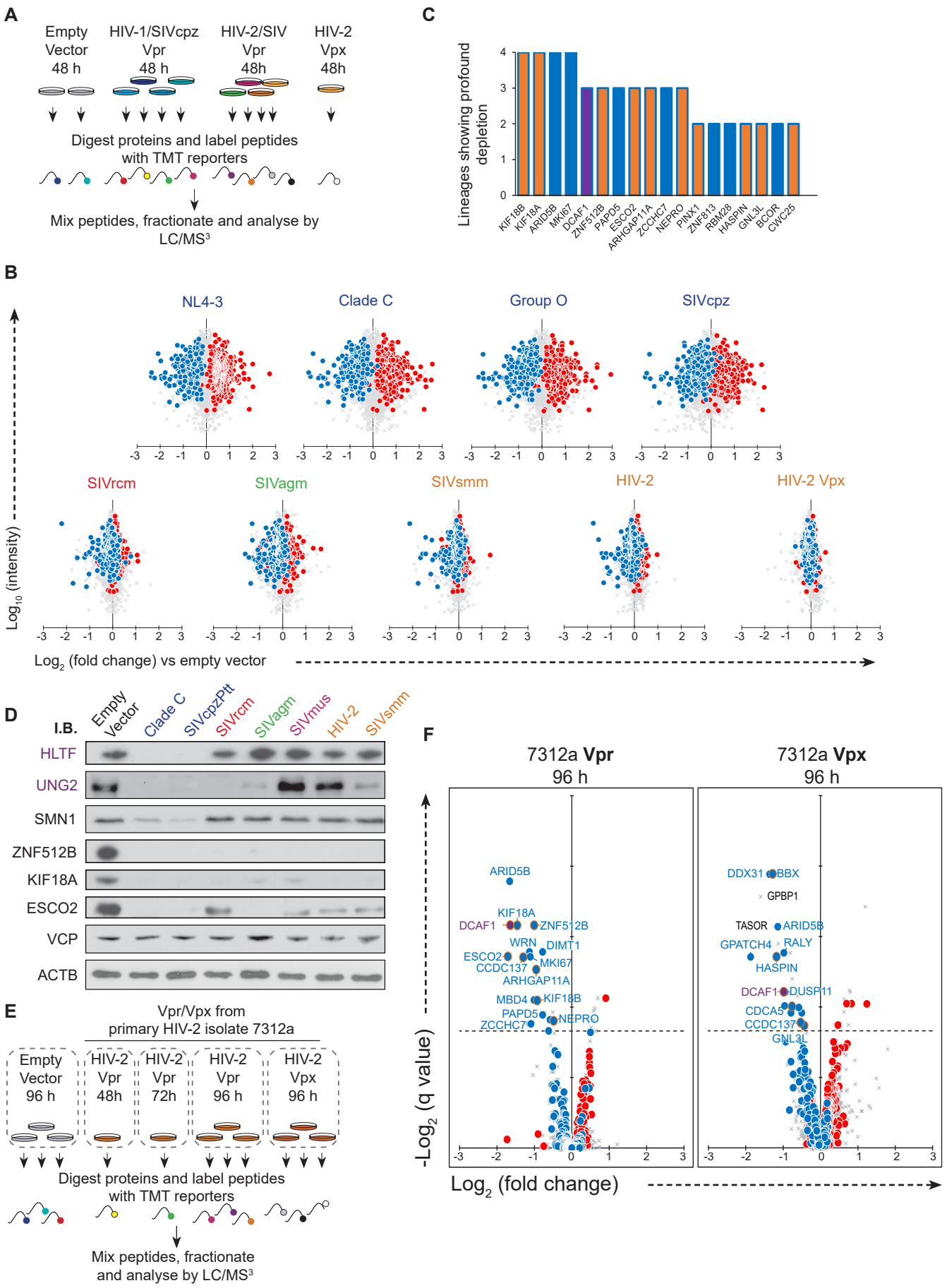
A
Empty Vector 48 h
HIV-1/SIVcpz Vpr 48 h
HIV-2/SIV Vpr 48h
HIV-2 Vpx 48h
Digest proteins and label peptides with TMT reporters
Mix peptides, fractionate and analyse by LC/MS³
C
Lineages showing profound depletion
KIF18B
KIF18A
ARID5B
MKI67
DCAF1
ZNF512B
PAPD5
ESCO2
ARHGAP11A
ZCCHC7
NEPRO
PINX1
ZNF813
RBM28
HASPIN
GNL3L
BCOR
CWC25
B
NL4-3
Clade C
Group O
SIVcpz
SIVrcm
SIVagm
SIVsmm
HIV-2
HIV-2 Vpx
Log10 (intensity)
Log2 (fold change) vs empty vector
D
I.B.
Empty Vector
Clade C
SIVcpzPtt
SIVrcm
SIVagm
SIVmus
HIV-2
SIVsmm
HLTF
UNG2
SMN1
ZNF512B
KIF18A
ESCO2
VCP
ACTB
E
Vpr/Vpx from primary HIV-2 isolate 7312a
Empty Vector 96 h
HIV-2 Vpr 48h
HIV-2 Vpr 72h
HIV-2 Vpr 96 h
HIV-2 Vpx 96 h
Digest proteins and label peptides with TMT reporters
Mix peptides, fractionate and analyse by LC/MS³
F
7312a Vpr 96 h
7312a Vpx 96 h
ARID5B
KIF18A
DCAF1
ZNF512B
WRN
DIMT1
ESCO2
MKI67
CCDC137
ARHGAP11A
MBD4
KIF18B
PAPD5
NEPRO
ZCCHC7
DDX31
BBX
GPBP1
TASOR
ARID5B
GPATCH4
RALY
HASPIN
DCAF1
DUSP11
CDCA5
CCDC137
GNL3L
-Log2 (q value)
Log2 (fold change)

760 ## Supplemental Information

761 **Table S1. Interactive database of protein changes in the datasets presented here.**

762 **Figure S1 – Related to Figure 2. Immunoblot replication of proteins altered by Vpr and additional**
763 **information relating to experiment described in Figure 2.**

764 **A,** Scatterplots displaying pairwise comparisons between WT, ΔVpr and mock-infected cells. Vpr
765 depleted proteins confirmed by blot in this figure are highlighted in blue, UNG, ZGPAT and HLTF are
766 previously identified targets for Vpr mediated degradation, shown in purple. CCNB1 is increased by
767 Vpr (red). **B,** Scatterplot displaying pairwise comparison between cells exposed to empty or Vpr
768 bearing viral particles. **C,** Immunoblot of proteins highlighted in this figure. **D,** Immunoblot of
769 purified virus preparations used to infect cells for the proteomics experiment displayed in **Fig 2A**. **B,**
770 Bar chart showing the average scaled abundance of matrix, capsid and integrase peptides detected
771 in the cell lysate by MS. Bars show mean and standard deviation. **E,** 7-AAD stain of cells exposed to
772 empty vector, or Vpr wild type or Vpr mutants. Watson pragmatic modelling was used to identify
773 cells in G1 (blue), S (grey) or G2/M (red) phase. **F**, Heatmap showing the behaviour of the 100
774 proteins most depleted by Vpr particles (blue) and increased (red) within the defined highly
775 modulated subsets. Colour indicates the $\log_2$ fold change of each protein in each condition
776 compared to empty particle treatment. Genes were clustered using uncentered Pearson correlation
777 and centroid linkage, and conditions clustered by column means. **G,** Defined groups of Vpr depleted
778 and increased proteins were subject to gene ontology enrichment analysis, compared with a
779 background of all proteins quantitated in these experiments. Plots show all significantly enriched
780 (Fisher's exact test with Bonferroni correction) molecular function terms with associated p values. +
781 / - indicates if the classification was enriched or de-enriched compared with the expected number of
782 proteins expected by chance. Where significant, associated p value represents the results of a
783 Fisher's exact test with Bonferroni correction. This is highly conservative as it is corrected for all
784 1061 possible cellular compartment terms, not just those shown.

785 **Figure S2 – Related to Figure 2. Quantifying the effect of Vpr under reduced DCAF1 conditions.**

786 **A,** Graphical summary of the DCAF1 KD experiment. **B,** Scatterplot displaying pairwise comparison
787 between Sh-Control and Sh-DCAF1 cells at 0 h, with defined groups of 302 Vpr depleted (blue) and
788 413 increased (red) proteins highlighted. DCAF1 is highlighted in purple. **C,** Example time-course
789 behaviour for one Vpr target (HLTF) and one secondary Vpr effect (CCNB1). **D,** Scatterplots showing
790 the pairwise comparison between the 6 or 24 h time-point with the 0 h condition for each sh-
791 transduced cell line.

792 **Figure S3 – Related to Figure 2. Cell cycle regulation of Vpr modulated proteins.**

793 **A,** Ly, 2015 contains a proteomic analysis of NB4 cells treated with RO-3306 cells arrested in G2/M
794 with the PLK1 inhibtor RO-3306. Scatterplot showing the pairwise comparison of abundance of
795 proteins isolated from RO-3306 treated vs mock treated cells. Groups of proteins defined in the
796 current study of 302 Vpr depleted (blue) and 413 increased (red) proteins are highlighted, indicating
797 the behaviour of these proteins in NB4 cells arrested at G2/M. **B,** Correlation of the Vpr mediated
798 change in cyclin abundance in the present study (x-axis), with RO-3306 mediated changes in NB4
799 cells in Ly, 2015. Changes in cyclin abundance in HIV infection are assumed to be secondary to cell
800 cycle arrest, and thus this correlation indicates the concordance between effects secondary to cell

cycle arrest between the two datasets. **C,** Pie charts showing the overlap between changes in the present study and changes induced by G2/M arrest in Ly, 2015. Left panel shows the behaviour of all proteins quantified in both the present study (**Figure 1A** and **Figure 2A**) and Ly, 2015, i.e. a total of 1643 proteins were quantified in both datasets, of which 1100 proteins did not significantly change in G2/M arrest, 260 proteins were significantly depleted in G2/M arrested cells, and 283 proteins were significantly increased in G2/M arrested cells. Middle panel shows the behaviour the defined group of 302 Vpr depleted proteins. I.e. of 302 proteins, a total of 90 proteins were detected in Ly, 2015, 58 of which did not significantly change in G2/M arrest, 18 were significantly depleted in G2/M arrest and 14 were significantly increased in G2/M arrest. † Indicates the fraction in each case where the change induced by cell cycle arrest is in the same direction as the effect of Vpr, i.e. the fraction for which cell cycle arrest could explain the Vpr mediated protein changes. Right panel shows the behaviour of the defined group of 413 Vpr increased proteins. **D,** Fischer, 2016, define lists of 115 proteins whose expression peaks in G1/S phase and 174 proteins whose expression peaks in G2/M phase. Pie-charts show the overlap between these lists and (left) all proteins detected in the present study, (middle) proteins defined as being depleted by Vpr, and (right) proteins defined as being increased by Vpr. As in the proteomics dataset, there is some enrichment of proteins with peak expression in G2/M within Vpr increased proteins, and some enrichment of proteins with peak expression in G1/S in Vpr depleted proteins, consistent with some effects being secondary to cell cycle arrest, but these effects are in the minority.

Figure S4 – Related to Figure 3. MS-IP approach to identify direct targets for Vpr mediated degradation.

A, Graphical summary of the MS-IP experiment. All cells were stably transduced with an ShDCAF1 vector as described earlier. MLN4924 is a pan-Cullin inhibitor. **B,** 20 most abundant proteins identified by Co-IP determined by number of unique peptides, normalised as a proportion of the maximum possible peptide count for each protein, (Exponentially modified protein abundance index, emPAI). Proteins falling within the defined list of 302 Vpr depleted and 413 Vpr increased proteins are highlighted in blue and red respectively. **C,** The same 20 proteins with signal intensity rather than peptide number shown. **D,** Pie chart indicating the overlap between the proteins co-immunoprecipitated with Vpr and the defined list of 302 Vpr decreased (blue) and 413 Vpr increased proteins (red), and proteins detected but falling into neither list (grey). **E**, Bar chart showing the enrichment of Vpr depleted and Vpr increased proteins within proteins co-immunoprecipitated with Vpr compared to the expected numbers of proteins that would be co-immunopreciptated from each group by chance. p value indicates a Fisher's exact test of a 2x2 contingency table (Vpr depleted/increased, identified by co-IP/not identified), indicating that the two criteria are significantly linked.

Figure S4 – Related to Figure 5. Additional information relating to expanded panel of primate lentiviral Vpr and Vpx varients & Depletion of HuSH components by lentiviral Vpx and Vpr proteins.

A, %GFP positive (transduced) cells at harvest. Cells were transduced at an infectious MOI of 1.5 based on prior titration, with the actual resulting % transduction varying slightly across the samples. **B**, Proportion of cells in G2/M at point of harvest based on 7-AAD staining and Watson pragmatic modelling. **C,** Scatterplots showing the pairwise comparison between each Vpr tested and empty vector control with HuSH complex components highlighted. **D**, Bar graph of GFP percentage positive

844 of JLAT-A1 cells after transduction with control (Cre recombinase), Vpr or Vpx proteins and
845 treatment with TNFα. Mean and SEM of 3 biological replicates per condition are shown,
846 representative of three independent similar experiments. p-values determined by ordinary one-way
847 ANOVA with Bonferroni comparison between Vpr/Vpx treatment and control treated cells. **E,**
848 Phylogenetic tree of primate lentiviruses based on an alignment of Vif nucleic acid sequences, with 5
849 major lineages of primate lentiviruses labelled. Information on Vpr and Vpx activity based on a
850 selected number of isolates tested in each lineage in Lim, 2012 (Lim et al., 2012) **F,** Immunoblot of
851 TASOR in cells transduced with a panel of Vpx and Vpr proteins.

Figure S1 - Related to Figure 2

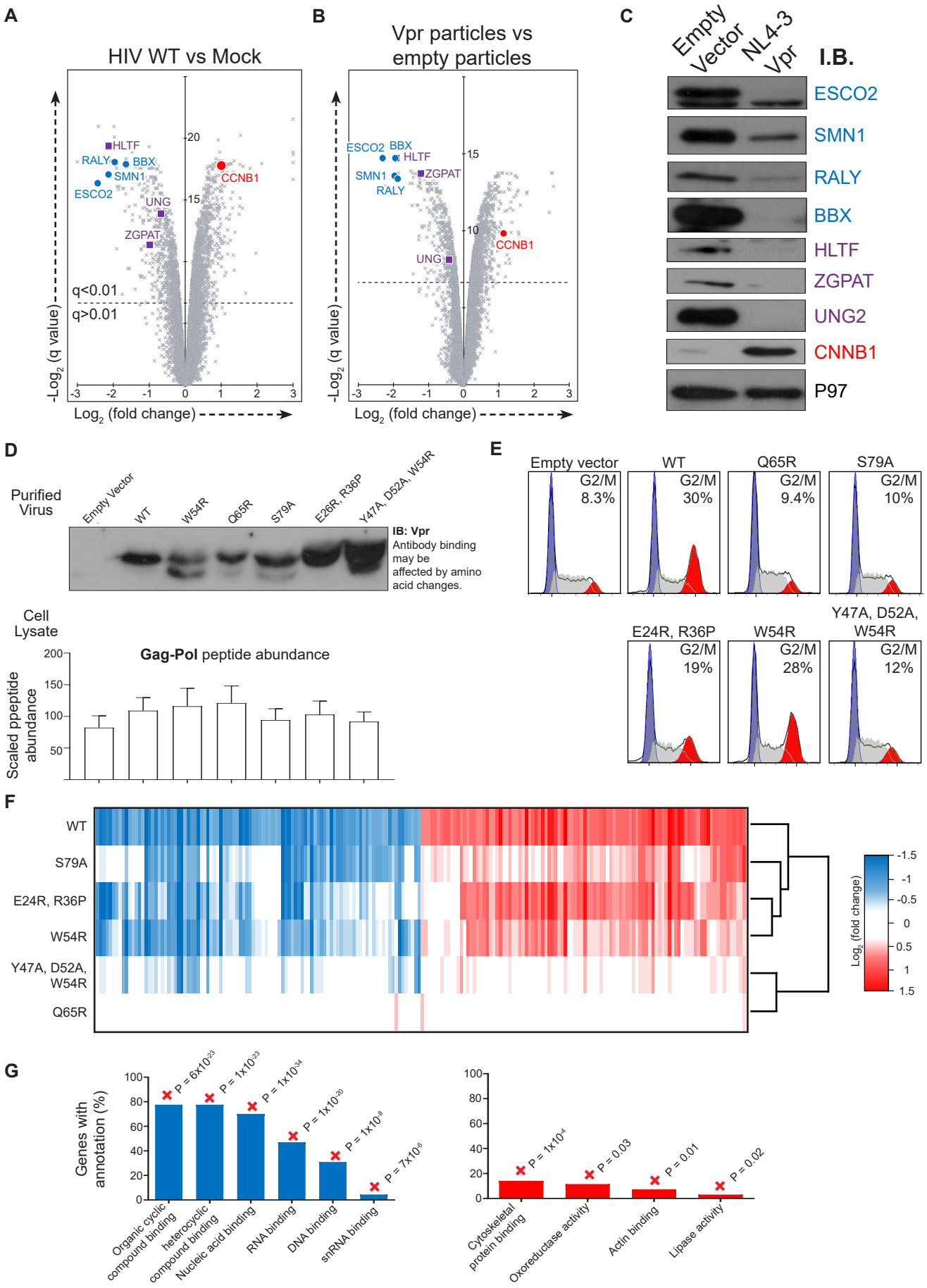

Figure S2 - Related to Figure 2

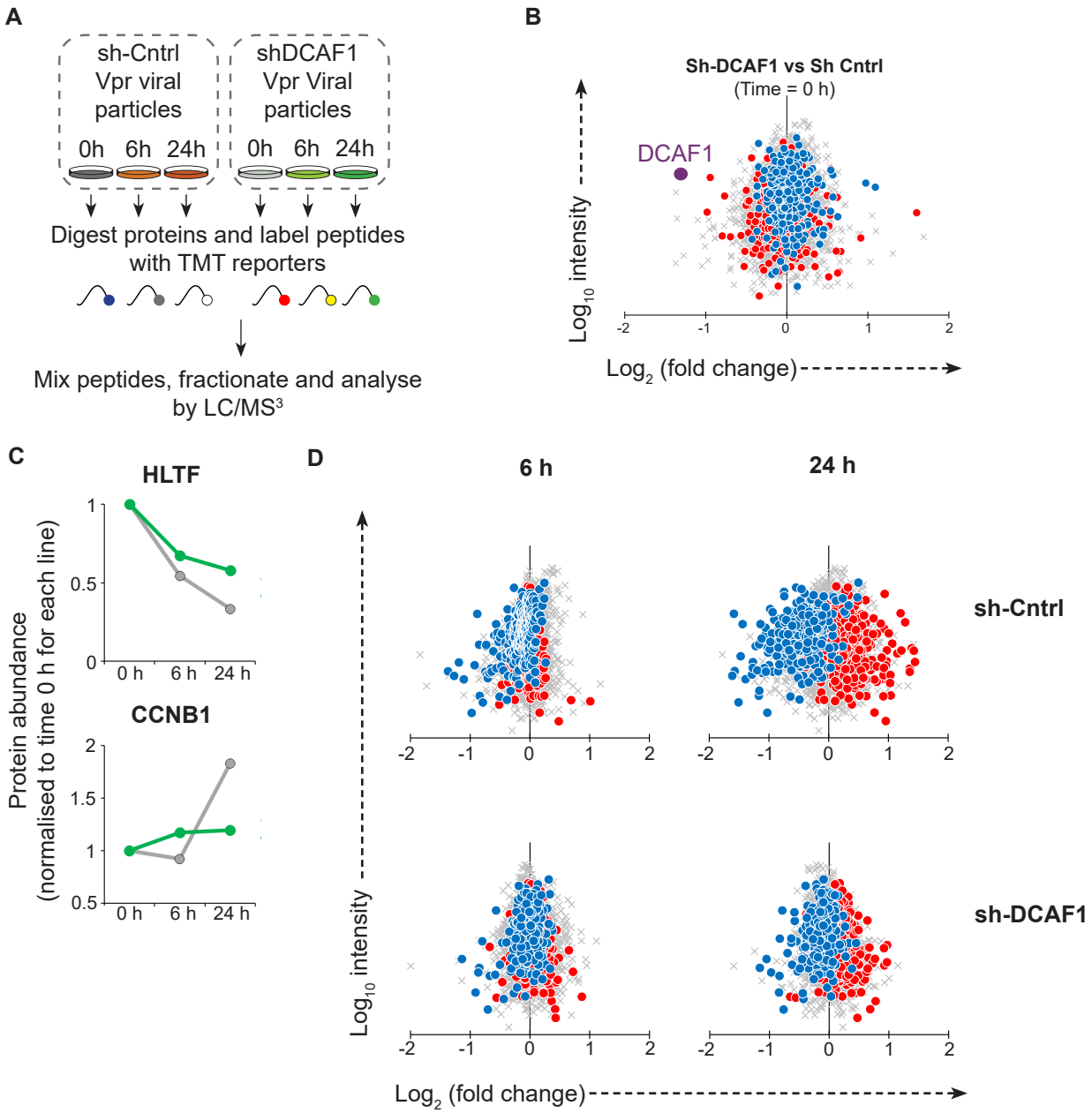

Figure S3, related to Figure 2

A Ly, 2015, Proteomics of cells arrested at G2/M using PLK1 inhibitor RO-3306

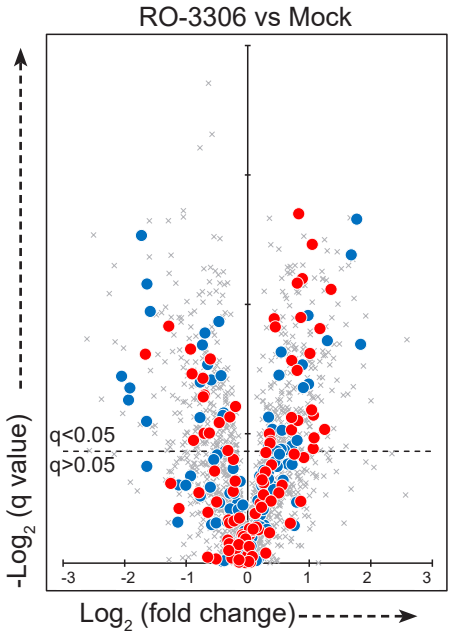

B

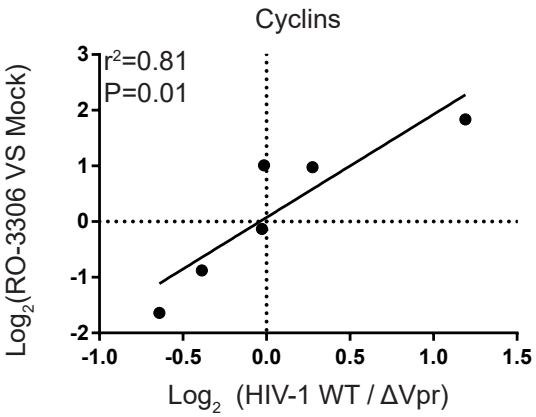

C

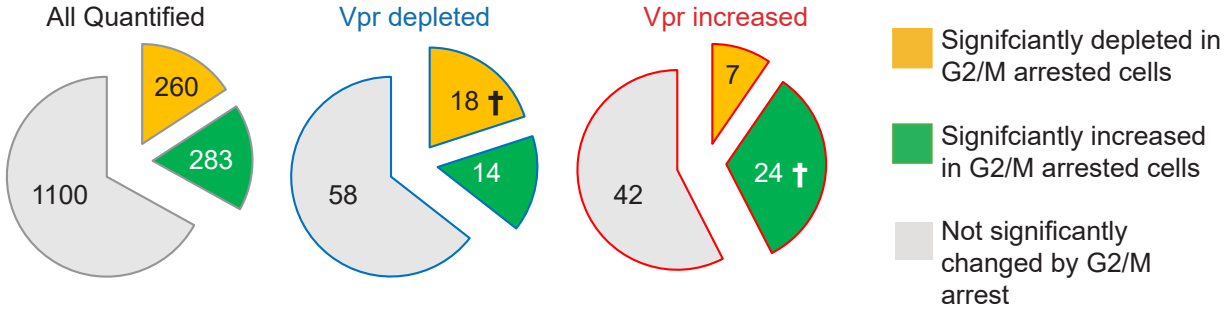

D Fischer, 2016 - Transcriptional anlalysis

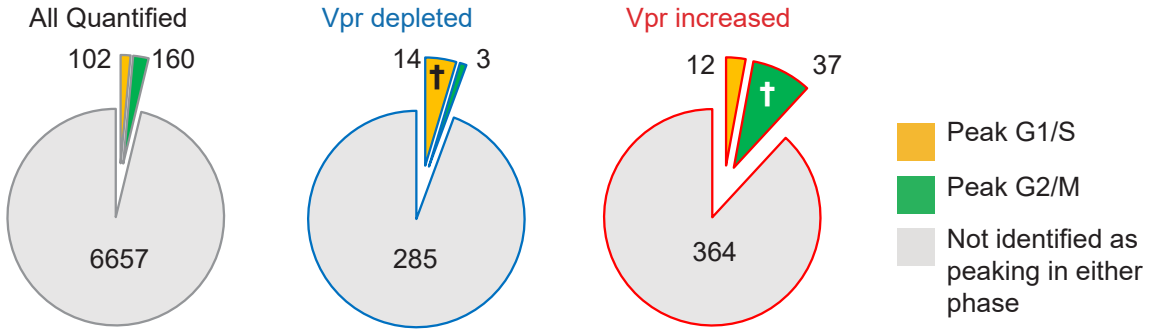

Figure S4 - Related to Figure 3

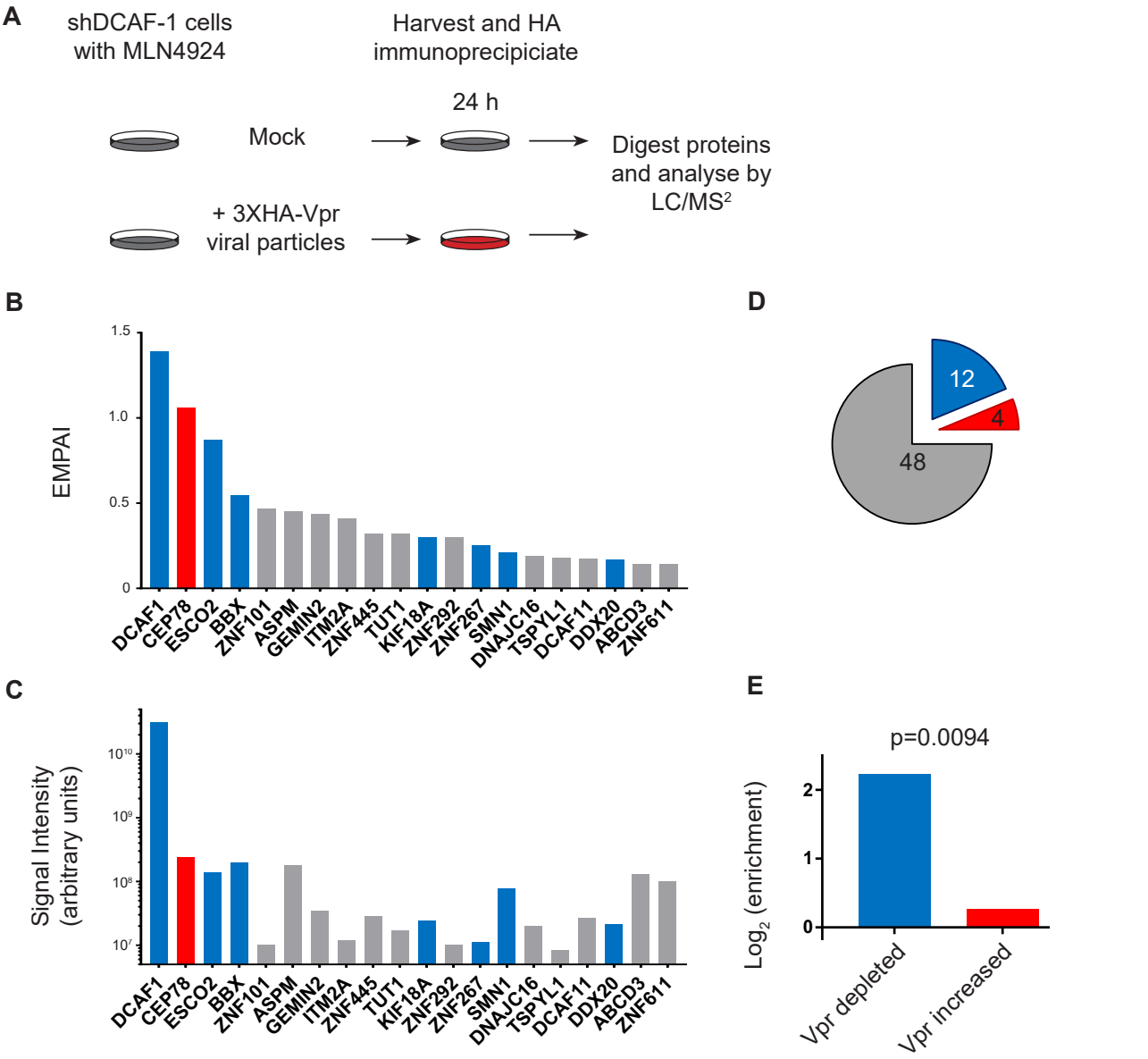

F

Accession	Gene	Vpr necessary	Incoming Vpr sufficient	Degraded within 6 h	Co-IP	In direct target list (Fig. 3d)?
Q14527	HLTF	Yes	Yes	Yes	-	Yes
Q7L590	MCM10	Yes	Yes	ND	-	No - Not detected in 6 hour pulsed SILAC or IP
Q8N5A5	ZGPAT	Yes	Yes	Yes	-	Yes
Q96AY2	EME1	Yes	Yes	NS	-	No - depleted but with a Sig.B value of >0.01 in the pulsed SILAC experiment, not detected in IP
Q96NY9	MUS81	Yes	Yes	Yes	-	Yes
Q6N021	TET2	Yes	ND	ND	-	No - Not detected in incoming Vpr experiment (Fig. 2a)
P13051	UNG	Yes	Yes	NS	-	No - depleted but with a Sig.B value of >0.01 in the pulsed SILAC experiment. Detected in the Co-IP but with a single peptide

Figure S5 - Related to Figure 5

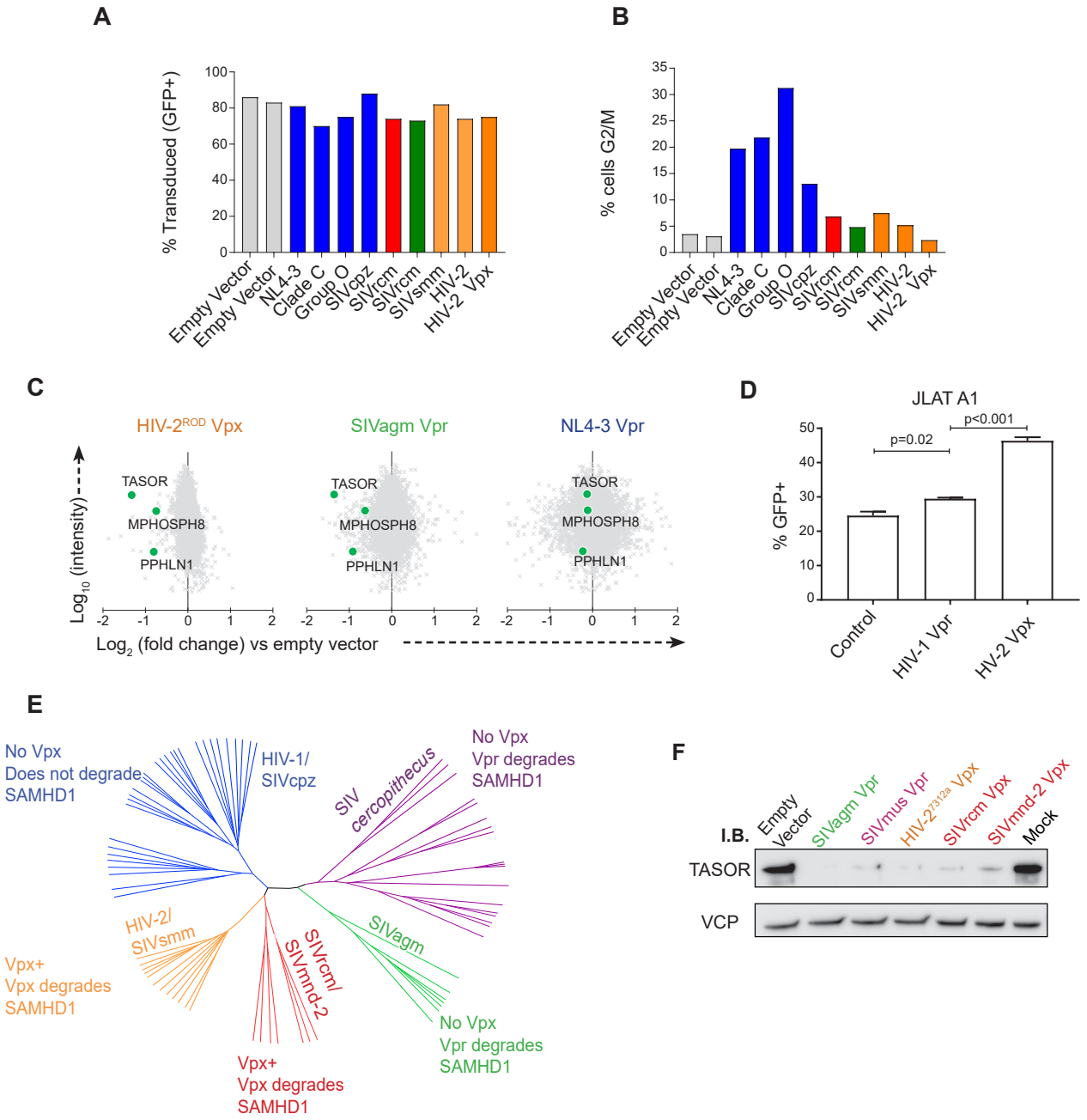

Table S2 – Related to Figure 5.

Vpr and Vpx variants used in this study.

Vpr **Species**	**Genbank** **Accession**	**Data presented in:**
HIV-1 $_{NL4-3}$	AF324493.2(Adachi et al., 1986)	Figures 1-5.
HIV-1 $_{98BR004}$ (Clade C)	AAK31002.1(Rodenburg et al., 2001)	TMT Proteomics experiment & IB (Figure 5A-D)
HIV-1 $_{BCF09}$ (Group O)	CAA75954.1	TMT Proteomics experiment (Figure 5A-C)
SIVcpzPtt $_{MB897}$	ABU53019.1(Van Heuverswyn et al., 2007)	TMT Proteomics experiment & IB (Figure 5A-D)
SIVrcm $_{02CM8081}$	ADK78264.1(Ahuka-Mundeke et al., 2010)	TMT Proteomics experiment & IB (Figure 5A-D)
SIVagm $_{Sab92018}$	ADO34202.1(Gnanadurai et al., 2010)	TMT Proteomics experiment & IB (Figure 5A-D), I.B, (Figure S5F)
SIVsmm $_{E660}$	ANT86736.1(Lopker et al., 2016)	TMT Proteomics experiment & IB (Figure 5A-D)
HIV-2 $_{ROD}$	CAA28911.1(Guyader et al., 1987)	TMT Proteomics experiment (Figure 5A-C)
HIV-2 $_{7312a}$	AAL31354.1	I.B. (Figure 5D), Proteomics experiment, (Figure 5E,F)
SIVmus $_{01CM1239}$	ABO61047.1(Aghokeng et al., 2007)	I.B. (Figure 5D), I.B. (Figure S5F)

Vpx

Species	**Genbank** **Accession**	**Data presented in:**
HIV-2 $_{ROD}$	AAB00766.1(Guyader et al., 1987)	Proteomics experiment (Figure 5A-C)
HIV-2 $_{7312a}$	AAL31353.1	I.B. (Fig.5D), I.B. (Fig. S5F), Proteomics experiment, (Figure 5E,F)
SIVrcm $_{Ng411}$	AAK69676.1(Beer et al., 2001)	I.B. (Fig. S5F)
SIVmnd-2 $_{5440}$	AAO22477.1 (Hu et al., 2003)	I.B. (Fig. S5F)

852

853

854 ## Supplemental Experimental Procedures

855 **Lentivector for shRNA expression**

856 For lentiviral shRNA-mediated knockdown of DCAF1 hairpins were cloned into pHRSIREN-PGK-hygro,
857 with transduced cells selected for hygromycin resistance.
858 The following oligonucleotide was inserted using BamHI-EcoRI (only top oligonucleotide shown),
859 identified from the Broad Institute GPP Web portal. Gene specific target sequence (forward and
860 reverse complement) is underlined.

861 **DCAF1**

862 GATCCGCTGAGAATACTCTTCAAGAATTCAAGAGATTCTTGAAGAGTATTCTCAGCTTTTTTG

863 The same methodology was used to clone other shRNA haripins, the forward orientation targeting
864 sequence used for each is shown below:

865

MCM10-1

AGATGCAGGAGCGCTACTTTG

MCM10-2

GACGGCGACGGTGAATCTTAT

CCNT1

GCCTGCATTTGACCACATTTA

PINX1

CCTTCAGCAAGAGAGTTTAAT

ZNF267-1

TACTCGTTCCTCCAATCTTAT

ZNF267-2

ATCAATATAGGAAGGTCTTTA

MBD1

CACCAACCTTCCAAGTGTAAA

KIF20A

CCGATGACGATGTCGTAGTTT

CWC25

GATCACAGAAGAAGATGGCA

ZNF574

ACCACCTTGTAAGTTCTAAAT

SMN1-1

ATCTGTGAAGTAGCTAATAA

SMN1-2

GGCTATCATACTGGCTATTAT

CDCA2 -1

AGACTGGGTTCAGGTTATTTC

CDCA2 -2

CCGTTCTCAGTTCTCCTAATA

DDX20

TCAGCTACTTATCCCGAATTT

ZNF316

CTTCCAAAGTGCTGGGATTAT

MSH6

AGGCGAAGTAGCCGCCAAATA

RFC1

CGCACTAATTATCAAGCTTAT

CDCA5

CGAGAAACAGAAACGTAAGAA

866

867 **Gene ontology enrichment analysis**

868 Analysis was carried out using Panther (Mi et al., 2017), using the web interface at:
869 http://pantherdb.org/. Lists of proteins highly significantly depleted or increased by Vpr were
870 compared to a background list of proteins quantified in the two experiments used to define those
871 lists.

872 **7-AAD staining**

873 Cells were fixed in ice cold 70% ethanol for at least 30 minutes, washed with PBS and stained in
874 25ug/ml 7-AAD for 15 minutes before acquisition on a BD FACSCalibur. Analysis was carried out in
875 Flowjo, v.10.5.2. Dead cells and doublets were excluded by gating on forward scatter, side scatter,
876 and fluorescent area and height. Univariate cell cycle modelling was carried out using the Watson
877 pragmatic method.

878 **ShRNA knockdown confirmation by RT-PCR**
879 Total RNA was extracted using the RNeasy Plus Mini kit (Qiagen). Total RNA (250 ng) was reverse
880 transcribed into cDNA using a poly(d)T primers and SuperScript III Reverse Transcriptase (Invitrogen)
881 following the manufacturer's instructions. Real-time qRT–PCR was performed using the ABI 7500
882 Real-Time PCR system (Applied Biosystems) and SYBR Green PCR Master Mix (Applied Biosystems),
883 with cycling parameters of 50°C for 2 min and 95°C for 5 min, followed by 40 cycles of 95°C for 15 s
884 and 60°C for 1 min. The gene-of-interest specific primer pairs were predesigned and purchased from
885 Sigma-Aldrich as KiCqStart primers, with the following sequences: MCM10_FOR 5'-
886 CTTATACAGAAGAGGCTGATG and MCM10_REV 5'-CCTCTTGCAACTCTTCATTC; ZNF267_FOR 5'-
887 GTAGAATTCTCTTTGGAGGAG and ZNF267_REV 5'-CTCACTCTTCACATTCCAAG; CDCA2_FOR 5'-
888 AGGAAAGTCATCATCCTACC and CDCA2_REV 5'-GATGGTTTGTTTCAGGAGAG; SMN1_FOR 5'-
889 GGAAAGCCAGGTCTAAAATTC and SMN1_REV 5'-AGAATCTGGACATATGGGAG. The difference in the
890 amount of input cDNA was normalized to an internal control of GAPDH, using the following primers:
891 GAPDH_FOR: 5' ATGGGGAAGGTGAAGGTCG and GAPDH_REV: 5'- CTCCACGACGTACTCAGCG.

892 **Mass spectrometry Immunoprecipitation (MS-IP)**
893 CEM-T4 T-cells were lysed in 1 % NP-40. Lysates were pre-cleared with IgG-Sepharose (GE
894 Healthcare, UK) and incubated for 3 hr at 4°C with anti-HA coupled to agarose beads (Sigma EZview
895 Red Anti-HA Affinity Gel). After washing in 0.5% NP-40, samples were eluted with 0.5 mg/ml HA
896 peptide at 37°C for 1 hr. Additional detail on MS methods is available at the end of this section.
897 Proteins defined as co-immunoprecipitating with Vpr were detected with at least 3 peptides in the
898 Vpr condition, not identified in the control condition, and were present in <20% of MS-IP available in
899 the Crapome (Mellacheruvu et al., 2013) database http://crapome.org/.

900 **Pulsed Stable isotope labelling with amino acids in cell culture (Pulsed-SILAC)**
901 For SILAC labelling, CEM-T4 T-cells were grown for at least 7 cell divisions in SILAC RPMI lacking
902 lysine and arginine (Thermo Scientific, Thermo Fisher Scientific, UK) supplemented with 10% dialysed
903 FCS (Gibco, Thermo Fisher Scientific), 100 units/ml penicillin and 0.1 mg/ml streptomycin, 280 mg/L
904 proline (Sigma, UK) and medium (K4, R6; Cambridge Isotope Laboratories, Tewksbury, MA) or heavy
905 (K8, R10; Cambridge Isotope Laboratories) $^{13}C/^{15}N$-containing lysine (K) and arginine (R) at 50 mg/L.
906 At 0 h, cells were washed in media containing only light (^{12}C /^{14}N) lysine and arginine and were
907 maintained in this media for the duration of the experiment. Additional detail on MS methods is
908 available at the end of this section.

909

910 **J-LAT reactivation experiments.**

911 JLAT A1 cells were transduced with Cre recombinase, NL4-3 Vpr or HIV-2 ROD Vpx within a pHRSIN
912 IRES NGFR vector (Matheson et al., 2014). 24 h after transduction, cells were treated with 2 ng/ml
913 TNFα (PeproTech, 300-01A). After an additional 24 h cells were stained with anti-NGFR APC and
914 analysed for APC and GFP expression by flow cytometry. Cells were gated for NGFR+ cells to exclude
915 non-transduced cells. Flow cytometry data was acquired on a BD FACSCalibur.

916 **Phylogenetic tree of Vpr sequences.**

917 An existing nucleic acid sequence alignment of 191 representative Vif sequences from HIV-1, HIV-2
918 and SIVs from 22 primate species was downloaded from:

919 https://www.hiv.lanl.gov/content/sequence/NEWALIGN/align.html

920 A tree was generated using the percentage identity average distance in jalview (Waterhouse et al.,
921 2009) and visualised in Figtree:

922 http://tree.bio.ed.ac.uk/software/figtree/

923 10 sequences from 5 primate species not falling into the 5 highlighted linages are not shown.

924 **Sample Preparation for Mass spectrometry**

925 Samples were prepared using three different methods depending on the experiment. Initial infection
926 experiment was by SDC-FASP. VLP and shRNA experiments were by PreOmics NHS-iST sample
927 preparation Kit. pSILAC and MS-IP experiments were by SP3.

928 *SDC-FASP*

929 Samples prepared essentially according to the protocol in Leon *et al*(Leon et al., 2013). Briefly samples
930 were lysed in 50mM TEAB (pH8.5) 2% SDS, reduced and alkylated with TCEP/Iodoacetamide,
931 quantified by BCA assay. 50ug of each sample was diluted with TEAB/8M urea for loading onto 30kDa
932 ultrafiltration devices. Samples were washed 3 times with 500uL urea buffer and 3 times with
933 digestion buffer (TEAB/0.5% sodium deoxycholate) before resuspending in 50uL digestion buffer
934 containing 1ug trypsin and incubating overnight at 37 degrees. After digestion samples were spun
935 through the filters and filters washed with 50uL TEAB. SDC was removed by acidification and two
936 phase partitioning with ethyl acetate before vacuum drying and labelling with TMT reagents according
937 to the manufacturer's instructions.

938 *PreOmics iST*

939 Samples lysed in kit lysis buffer and quantified by BCA assay. 25ug of each sample was digested
940 essentially according to manufacturer's instructions, scaling volumes for a digestion of 25ug total
941 protein.

942 *SP3*

943 Samples were lysed in 50mM TEAB (pH8.5) 2% SDS (MS-IPs were adjusted to 2% SDS), reduced and
944 alkylated with TCEP/Iodoacetamide before digestion using the SP3 method(Hughes et al., 2014).
945 Briefly, carboxylate modified paramagnetic beads are added to the sample and protein is bound to
946 the beads by acidification with formic acid and addition of acetonitrile (ACN, final 50%). The beads are
947 then washed sequentially with 100% ACN, 70% Ethanol (twice) and 100% ACN. 10-20uL TEAB

948 (Triethylammonium bicarbonate) pH8 and 0.1% Sodium deoxycholate (SDC) is then added to the
949 washed beads along with trypsin. Samples were then incubated overnight at 37 degrees with periodic
950 shaking at 2000rpm. After digestion, peptides are immobilised on beads by addition of 200-400uL ACN
951 and washed twice with 100uL ACN before eluting in 19uL 2% DMSO and removing the eluted peptide
952 from the beads.

953 **Off-line high pH reversed-phase (HpRP) peptide fractionation**

954 For whole cell proteome samples HpRP fractionation was conducted on an Ultimate 3000 UHPLC
955 system (Thermo Scientific) equipped with a 2.1 mm × 15 cm, 1.7µ Aqcuity BEH C18 column (Waters,
956 UK). Solvent A was 3% ACN, Solvent B was 100% ACN, solvent C was 200 mM ammonium formate (pH
957 10). Throughout the analysis solvent C was kept at a constant 10%. The flow rate was 400 µL/min and
958 UV was monitored at 280 nm. Samples were loaded in 90% A for 10 min before a gradient elution of
959 0–10% B over 10 min (curve 3), 10-34% B over 21 min (curve 5), 34-50% B over 5 mins (curve 5)
960 followed by a 10 min wash with 90% B. 15 s (100 µL) fractions were collected throughout the run.
961 Peptide containing fractions were orthogonally recombined into 24 fractions (i.e. fractions 1, 25, 49,
962 73, 97 combined) and dried in a vacuum centrifuge. Fractions were stored at −80°C prior to analysis.

963 **Mass spectrometry**

964 Data were acquired on an Orbitrap Fusion mass spectrometer (Thermo Scientific) coupled to an
965 Ultimate 3000 RSLC nano UHPLC (Thermo Scientific). HpRP fractions were resuspended in 20 µl 5%
966 DMSO 0.5% TFA and 10uL injected. Fractions were loaded at 10 µl/min for 5 min on to an Acclaim
967 PepMap C18 cartridge trap column (300 um × 5 mm, 5 um particle size) in 0.1% TFA. After loading a
968 linear gradient of 3–32% solvent B was used for sample separation over a column of the same
969 stationary phase (75 µm × 50 cm, 2 µm particle size) before washing at 90% B and re-equilibration.
970 Solvents were A: 0.1% FA and B:ACN/0.1% FA. 3h gradients were used for whole cell proteomics
971 samples, 1h gradients for MS-IPs.

972 An SPS/MS3 acquisition was used for TMT experiments and was run as follows. MS1: Quadrupole
973 isolation, 120’000 resolution, 5e5 AGC target, 50 ms maximum injection time, ions injected for all
974 parallelisable time. MS2: Quadrupole isolation at an isolation width of m/z 0.7, CID fragmentation
975 (NCE 35) with the ion trap scanning out in rapid mode from m/z 120, 8e3 AGC target, 70 ms maximum
976 injection time, ions accumulated for all parallelisable time. In synchronous precursor selection mode
977 the top 10 MS2 ions were selected for HCD fragmentation (65NCE) and scanned out in the orbitrap at
978 50’000 resolution with an AGC target of 2e4 and a maximum accumulation time of 120 ms, ions were
979 not accumulated for all parallelisable time. The entire MS/MS/MS cycle had a target time of 3 s.
980 Dynamic exclusion was set to +/−10 ppm for 90 s, MS2 fragmentation was trigged on precursor ions
981 5e3 counts and above. For MS-IPs, MS2 instead used HCD fragmentation (NCE 34) and a maximum
982 injection time of 250ms and had a target cycle time of 2s. For pSILAC MS1 was acquired at 240’000
983 resolution.

984 **Data processing and analysis**

985 For TMT labelled samples data were searched by Mascot within Proteome Discoverer 2.1 in two
986 rounds of searching. First search was against the UniProt Human reference proteome (26/09/17), the
987 HIV proteome and compendium of common contaminants (GPM). The second search took all
988 unmatched spectra from the first search and searched against the human trEMBL database (Uniprot,

989 26/09/17). The following search parameters were used. MS1 Tol: 10 ppm, MS2 Tol: 0.6 Da. Enzyme:
990 Trypsin (/P). MS3 spectra were used for reporter ion based quantitation with a most confident
991 centroid tolerance of 20 ppm. PSM FDR was calculated using Mascot percolator and was controlled at
992 0.01% for 'high' confidence PSMs and 0.05% for 'medium' confidence PSMs. Normalisation was
993 automated and based on total s/n in each channel. Protein/peptide abundance was calculated and
994 output in terms of 'scaled' values, where the total s/n across all reporter channels is calculated and a
995 normalised contribution of each channel is output. Proteins/peptides satisfying at least a 'medium'
996 FDR confidence were taken forth to statistical analysis in R. This consisted of a moderated T-test
997 (Limma) with Benjamini-Hochberg correction for multiple hypotheses to provide a q value for each
998 comparison (Schwammle et al., 2013). MS-IPs were submitted to a similar search workflow with
999 quantitative data being derived from MS1 spectra via proteome discover minora feature detector
1000 node. For pSILAC experiments data were processed in MaxQuant and searched using Andromeda with
1001 similar search parameters (Cox and Mann, 2008). MaxQuant output was uploaded into Perseus for
1002 calculation of significance B (Tyanova et al., 2016). Where conditions were not carried out in triplicate,
1003 downstream analysis was limited to proteins identified with at least 3 unique peptides.

1004 **Supplemental References**

1005 Adachi, A., Gendelman, H.E., Koenig, S., Folks, T., Willey, R., Rabson, A., and Martin, M.A. (1986).
1006 Production of acquired immunodeficiency syndrome-associated retrovirus in human and nonhuman
1007 cells transfected with an infectious molecular clone. Journal of virology *59*, 284-291.
1008 Aghokeng, A.F., Bailes, E., Loul, S., Courgnaud, V., Mpoudi-Ngolle, E., Sharp, P.M., Delaporte, E., and
1009 Peeters, M. (2007). Full-length sequence analysis of SIVmus in wild populations of mustached
1010 monkeys (Cercopithecus cephus) from Cameroon provides evidence for two co-circulating SIVmus
1011 lineages. Virology *360*, 407-418.
1012 Ahuka-Mundeke, S., Liegeois, F., Ayouba, A., Foupouapouognini, Y., Nerrienet, E., Delaporte, E., and
1013 Peeters, M. (2010). Full-length genome sequence of a simian immunodeficiency virus (SIV) infecting
1014 a captive agile mangabey (Cercocebus agilis) is closely related to SIVrcm infecting wild red-capped
1015 mangabeys (Cercocebus torquatus) in Cameroon. The Journal of general virology *91*, 2959-2964.
1016 Beer, B.E., Foley, B.T., Kuiken, C.L., Tooze, Z., Goeken, R.M., Brown, C.R., Hu, J., St Claire, M., Korber,
1017 B.T., and Hirsch, V.M. (2001). Characterization of novel simian immunodeficiency viruses from red-
1018 capped mangabeys from Nigeria (SIVrcmNG409 and -NG411). Journal of virology *75*, 12014-12027.
1019 Cox, J., and Mann, M. (2008). MaxQuant enables high peptide identification rates, individualized
1020 p.p.b.-range mass accuracies and proteome-wide protein quantification. Nat Biotechnol *26*, 1367-
1021 1372.
1022 Gnanadurai, C.W., Pandrea, I., Parrish, N.F., Kraus, M.H., Learn, G.H., Salazar, M.G., Sauermann, U.,
1023 Topfer, K., Gautam, R., Munch, J.*, et al.* (2010). Genetic identity and biological phenotype of a
1024 transmitted/founder virus representative of nonpathogenic simian immunodeficiency virus infection
1025 in African green monkeys. Journal of virology *84*, 12245-12254.
1026 Guyader, M., Emerman, M., Sonigo, P., Clavel, F., Montagnier, L., and Alizon, M. (1987). Genome
1027 organization and transactivation of the human immunodeficiency virus type 2. Nature *326*, 662-669.
1028 Hu, J., Switzer, W.M., Foley, B.T., Robertson, D.L., Goeken, R.M., Korber, B.T., Hirsch, V.M., and Beer,
1029 B.E. (2003). Characterization and comparison of recombinant simian immunodeficiency virus from
1030 drill (Mandrillus leucophaeus) and mandrill (Mandrillus sphinx) isolates. Journal of virology *77*, 4867-
1031 4880.
1032 Hughes, C.S., Foehr, S., Garfield, D.A., Furlong, E.E., Steinmetz, L.M., and Krijgsveld, J. (2014).
1033 Ultrasensitive proteome analysis using paramagnetic bead technology. Mol Syst Biol *10*, 757.
1034 Leon, I.R., Schwammle, V., Jensen, O.N., and Sprenger, R.R. (2013). Quantitative assessment of in-
1035 solution digestion efficiency identifies optimal protocols for unbiased protein analysis. Mol Cell
1036 Proteomics *12*, 2992-3005.

1037 Lim, E.S., Fregoso, O.I., McCoy, C.O., Matsen, F.A., Malik, H.S., and Emerman, M. (2012). The ability
1038 of primate lentiviruses to degrade the monocyte restriction factor SAMHD1 preceded the birth of
1039 the viral accessory protein Vpx. Cell host & microbe *11*, 194-204.
1040 Lopker, M.J., Del Prete, G.Q., Estes, J.D., Li, H., Reid, C., Newman, L., Lipkey, L., Camus, C., Easlick,
1041 J.L., Wang, S.*, et al.* (2016). Derivation and Characterization of Pathogenic Transmitted/Founder
1042 Molecular Clones from Simian Immunodeficiency Virus SIVsmE660 and SIVmac251 following
1043 Mucosal Infection. Journal of virology *90*, 8435-8453.
1044 Matheson, N.J., Peden, A.A., and Lehner, P.J. (2014). Antibody-free magnetic cell sorting of
1045 genetically modified primary human CD4+ T cells by one-step streptavidin affinity purification. PLoS
1046 One *9*, e111437.
1047 Mellacheruvu, D., Wright, Z., Couzens, A.L., Lambert, J.P., St-Denis, N.A., Li, T., Miteva, Y.V., Hauri, S.,
1048 Sardiu, M.E., Low, T.Y.*, et al.* (2013). The CRAPome: a contaminant repository for affinity
1049 purification-mass spectrometry data. Nat Methods *10*, 730-736.
1050 Mi, H., Huang, X., Muruganujan, A., Tang, H., Mills, C., Kang, D., and Thomas, P.D. (2017). PANTHER
1051 version 11: expanded annotation data from Gene Ontology and Reactome pathways, and data
1052 analysis tool enhancements. Nucleic acids research *45*, D183-D189.
1053 Rodenburg, C.M., Li, Y., Trask, S.A., Chen, Y., Decker, J., Robertson, D.L., Kalish, M.L., Shaw, G.M.,
1054 Allen, S., Hahn, B.H.*, et al.* (2001). Near full-length clones and reference sequences for subtype C
1055 isolates of HIV type 1 from three different continents. AIDS Res Hum Retroviruses *17*, 161-168.
1056 Schwammle, V., Leon, I.R., and Jensen, O.N. (2013). Assessment and improvement of statistical tools
1057 for comparative proteomics analysis of sparse data sets with few experimental replicates. Journal of
1058 proteome research *12*, 3874-3883.
1059 Tyanova, S., Temu, T., Sinitcyn, P., Carlson, A., Hein, M.Y., Geiger, T., Mann, M., and Cox, J. (2016).
1060 The Perseus computational platform for comprehensive analysis of (prote)omics data. Nat Methods
1061 *13*, 731-740.
1062 Van Heuverswyn, F., Li, Y., Bailes, E., Neel, C., Lafay, B., Keele, B.F., Shaw, K.S., Takehisa, J., Kraus,
1063 M.H., Loul, S.*, et al.* (2007). Genetic diversity and phylogeographic clustering of SIVcpzPtt in wild
1064 chimpanzees in Cameroon. Virology *368*, 155-171.
1065 Waterhouse, A.M., Procter, J.B., Martin, D.M., Clamp, M., and Barton, G.J. (2009). Jalview Version 2--
1066 a multiple sequence alignment editor and analysis workbench. Bioinformatics *25*, 1189-1191.

1067